

# HRTEM Image Simulation

CCEM Summer School  
at McMaster University  
June 2 - 6, 2014

Pierre Stadelmann  
CIME-EPFL  
CH-1015 Lausanne  
Switzerland

June 3, 2014

- ▶ Why?
- ▶ How?
  - ▶ Methods.
  - ▶ Applications.

## Quantitative simulation?

- ▶ Problems.
- ▶ Perfect microscopes.
- ▶ Aberrations.

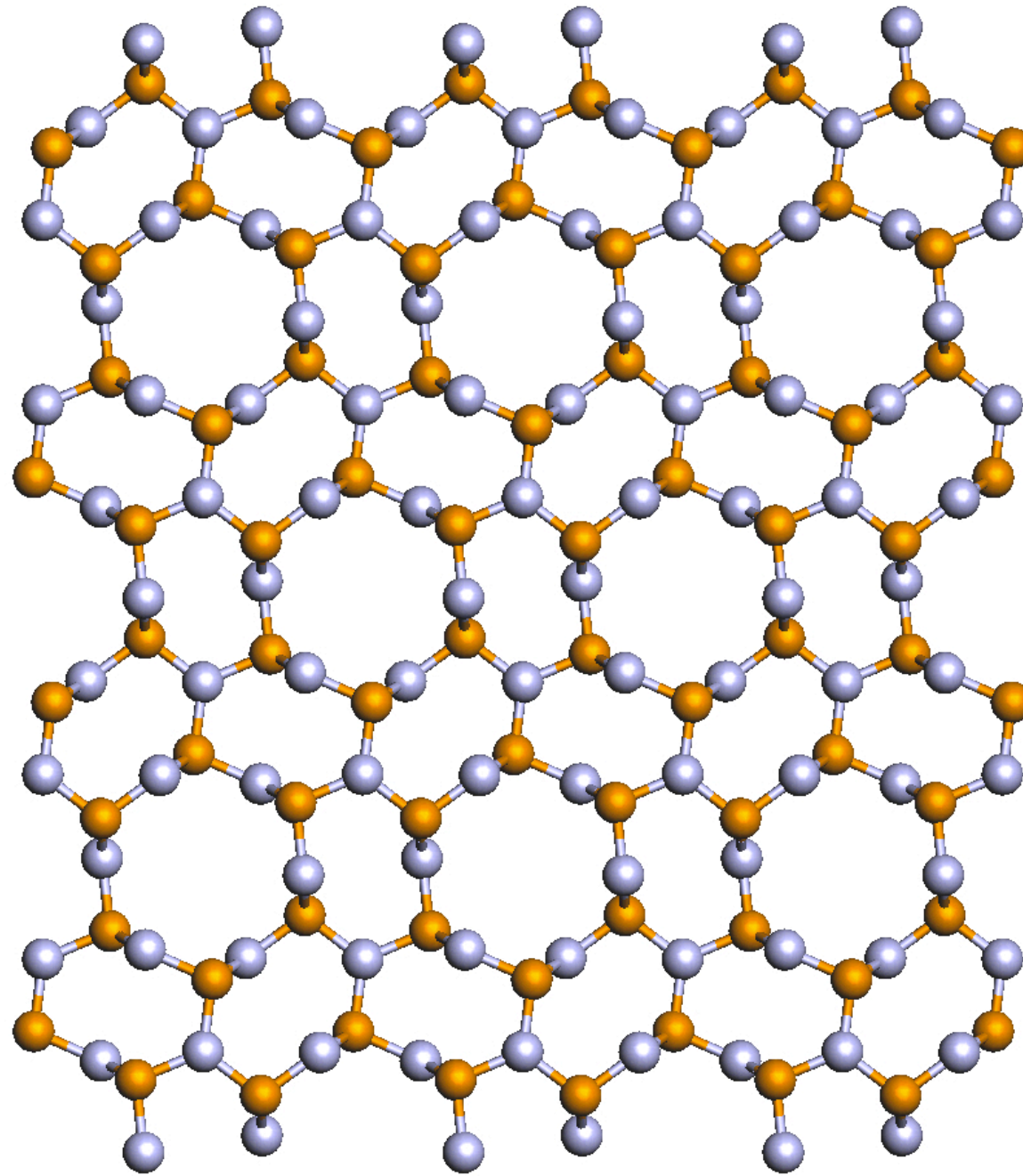
# Why HRTEM image simulation?

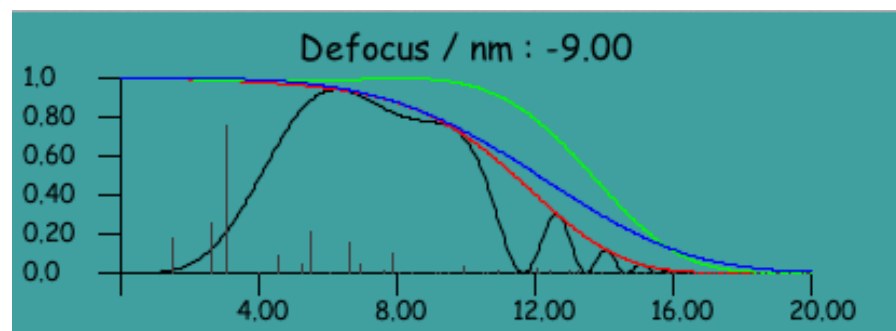
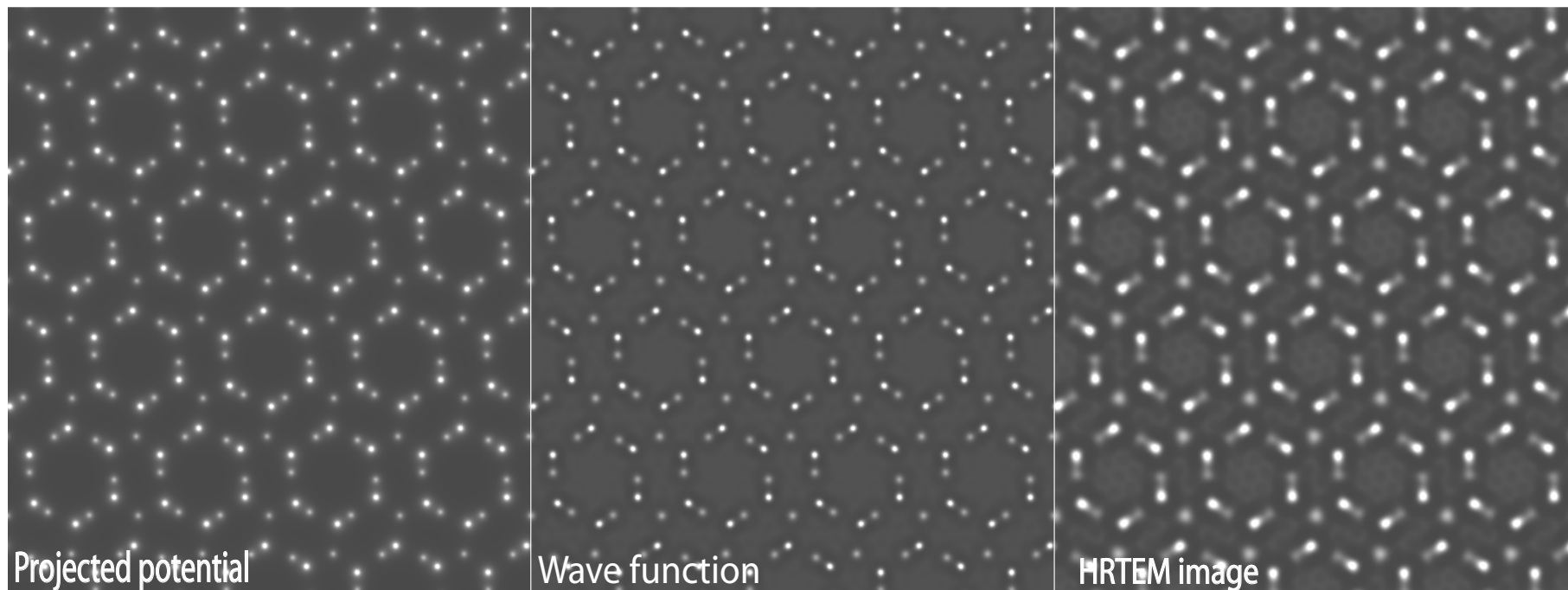
HR(S)TEM  $\implies$  to acquire knowledge on observed material (oriented in particular [uvw] directions):

- ▶ Specimen structure..
- ▶ Chemical composition.
- ▶ Functional properties.
- ▶ ...

But HR(S)TEM images depend of several adjustable microscope parameters.

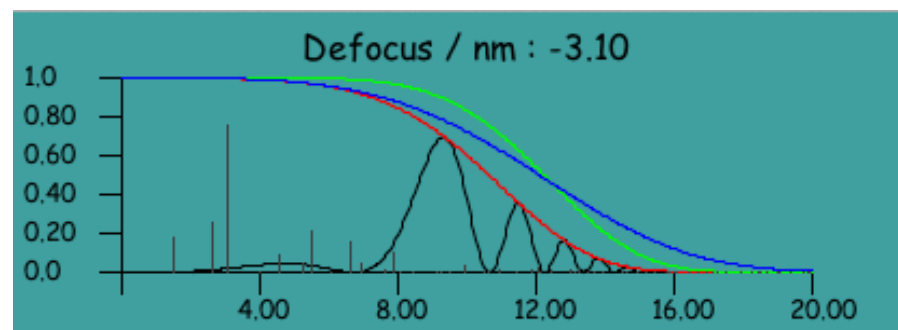
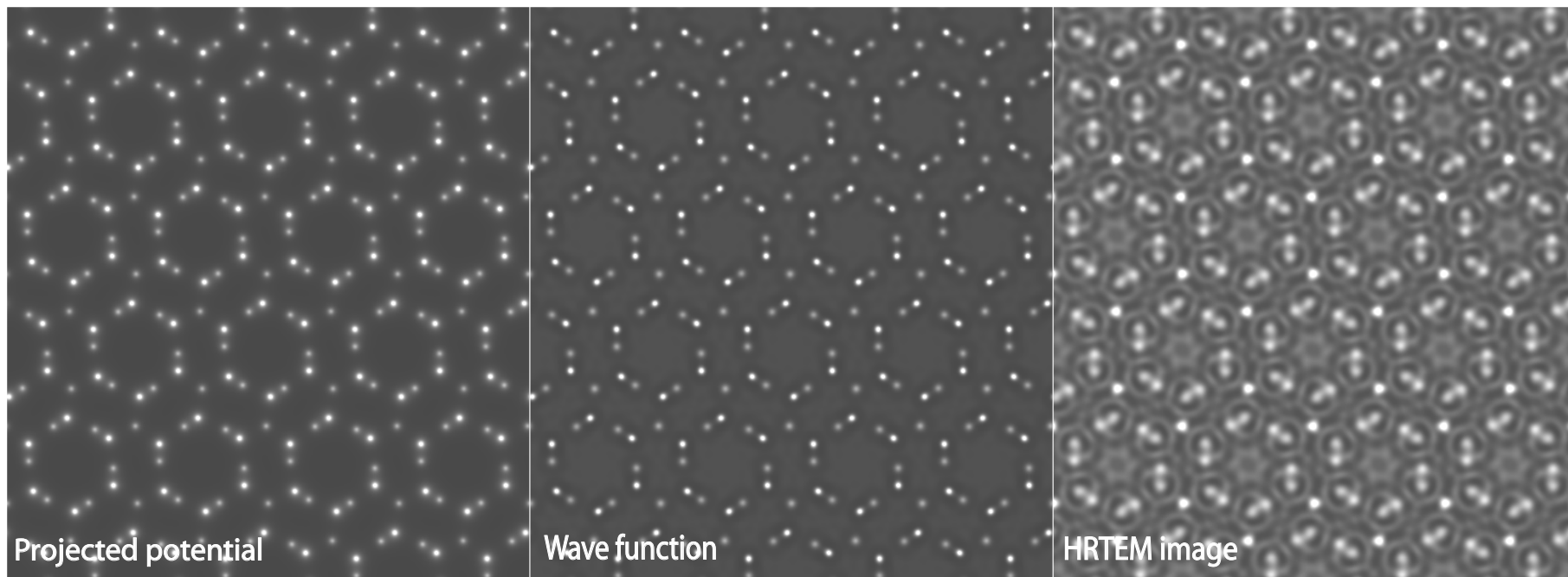
For example **object defocus** affects strongly HRTEM images.





Imaging parameters: Titan 80-300 (300 kV),  $C_s$  -0.033 mm

# $Si_3N_4$ P 63: [001], 10 nm thick, -3 nm defocus



Imaging parameters: Titan 80-300 (300 kV),  $C_s$  -0.033 mm

# How to do diffraction/image simulation?



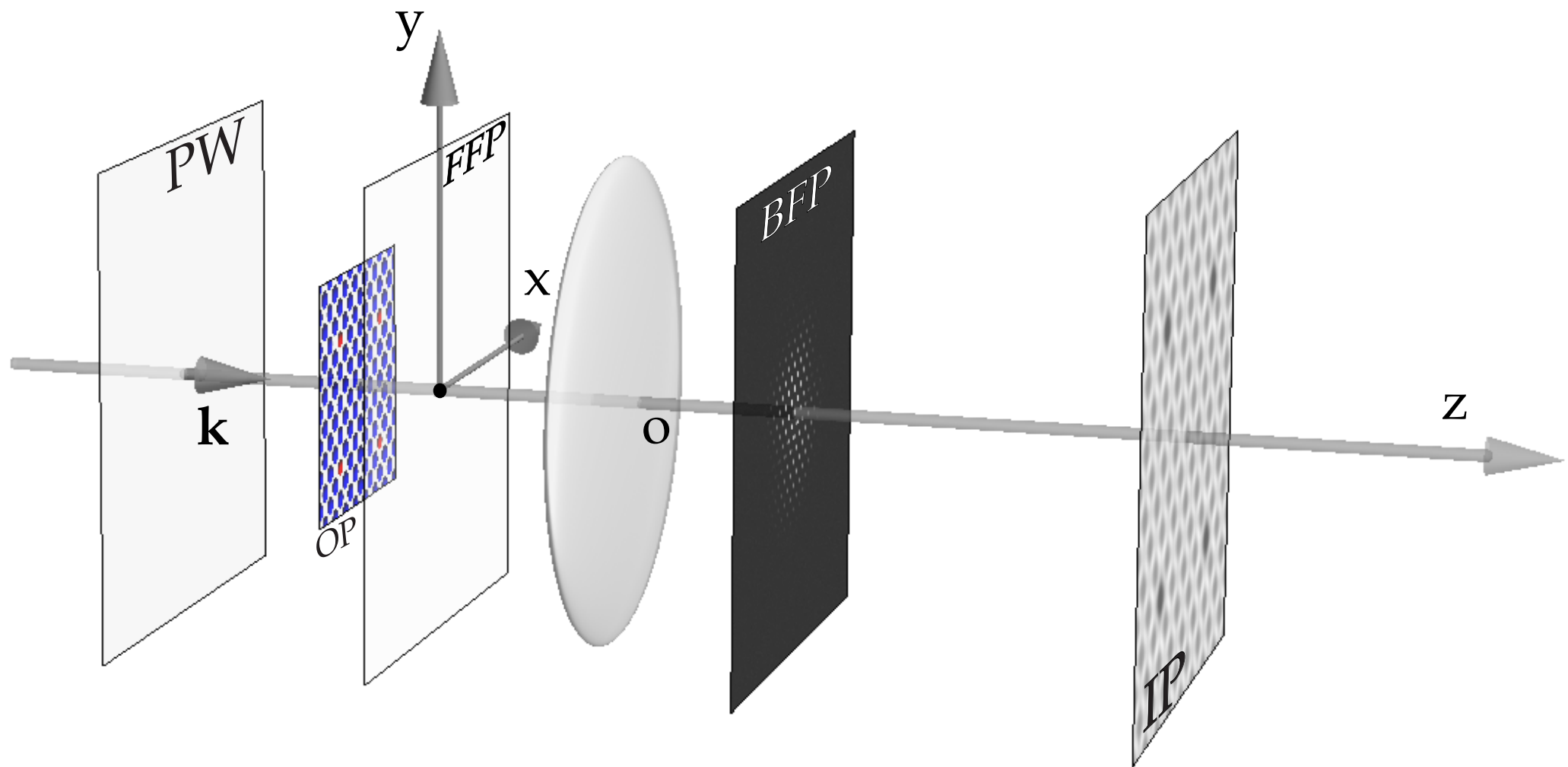
Formation of Electron Microscopy diffraction/images involves complex physical processes.

## Approximations and models of these physical processes

are required in order to perform computer simulations. Models are based on electron scattering, diffraction, optics, ...

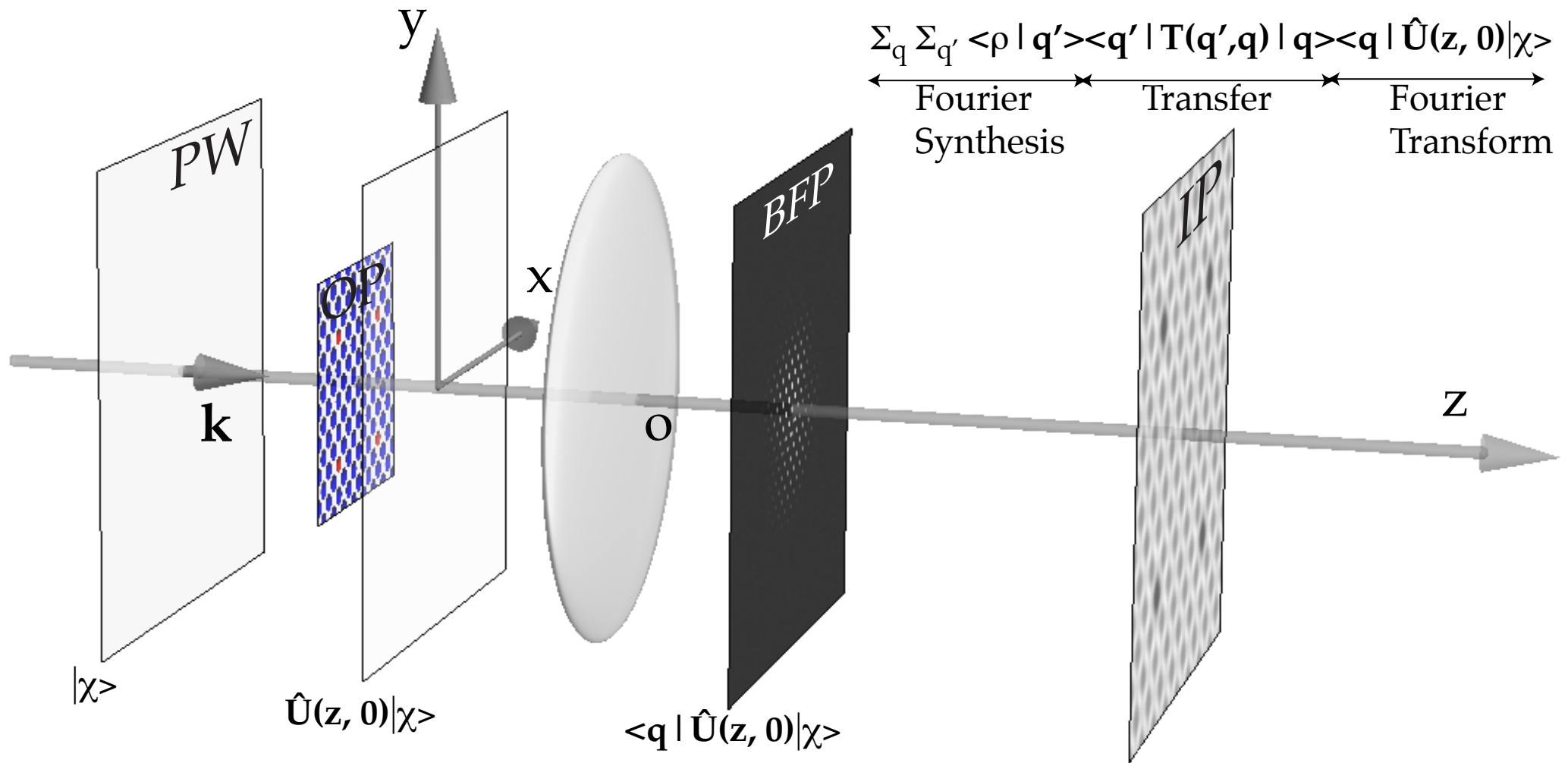
Needed: crystallography, optics, quantum mechanics, ... and computer programming.

# TEM (very) simplified model



Modeling steps: Incident wave (PW), crystal (OP), electron-matter interaction, Fraunhofer approximation, image formation (Abbe theory), ...

# Image formation modeling (HRTEM)



$|\chi\rangle \implies$  incident wave function

$$|\Psi_i\rangle = \underbrace{\sum_{q'} \langle \rho | q' \rangle}_{\text{Fourier synthesis}} \underbrace{\sum_q \langle q' | T(q', q) | q \rangle}_{\text{Objective lens transfer}} \underbrace{\langle q | U(z, 0) | \chi \rangle}_{\text{Fourier transform}}$$

Prior to perform any calculation the following items (from the electron source to the detector) must be characterized and modeled:

- ▶ The electron beam properties.
  - ▶ Convergence.
  - ▶ Source size.
  - ▶ Coherence (spatial and temporal).
- ▶ The specimen properties<sup>1</sup>.
- ▶ How is the incident electron beam scattered by the specimen?
- ▶ How does the microscope transfer the scattered electron beam?
- ▶ How do we measure the properties of the scattered electron beam (diffraction, image, hologram)?
- ▶ What are the properties of the detection system?

---

<sup>1</sup><file:///localhost/Applications/jemsMacOSX/html/Rb2W09/Rb2W09.html>

- ▶ Object.
- ▶ Scattering & diffraction.
- ▶ Image formation:
  - ▶ HRTEM.
  - ▶ HRSTEM.
- ▶ Image acquisition.

# Modeling the object

# Evolution operator $U(z, 0)$ defines the object properties

1. Amorphous material or crystalline material.
2. Thin or thick.
3. Orientation (high or low symmetry  $[uvw]$ ).

You might have to transform the unit cell in order to perform dynamical calculations<sup>2</sup>.

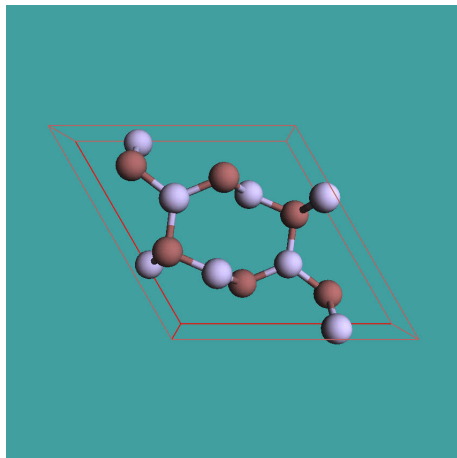


Figure:  $Si_3N_4$  hexagonal lattice.

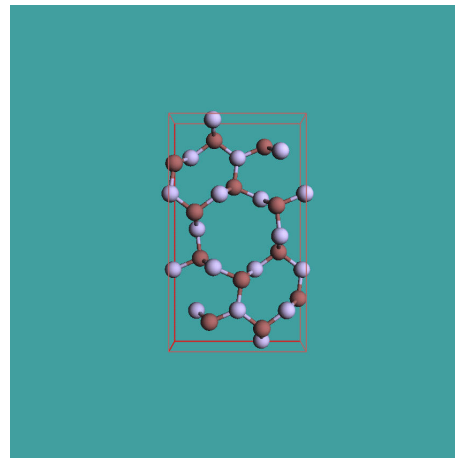


Figure:  $Si_3N_4$  orthorhombic lattice.

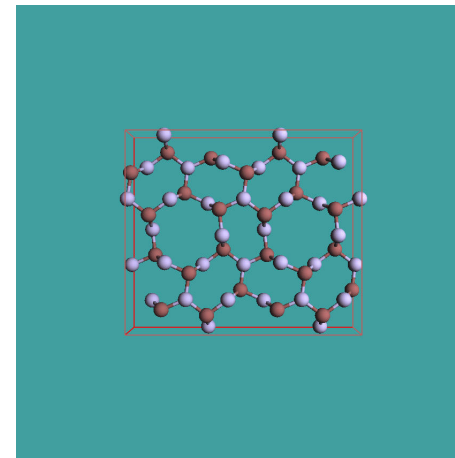


Figure:  $Si_3N_4$  orthorhombic lattice x 2.

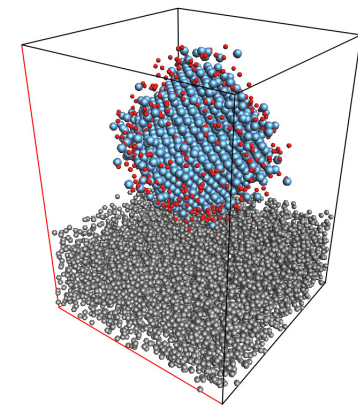


Figure: Pt catalyst on amorphous carbon film (9600 atoms).

Any model is considered a periodic unit cell independent of its complexity.

<sup>2</sup>See International Tables for Crystallography (1992) Vol. 1, Chapter 5.



# Atomic scattering amplitude

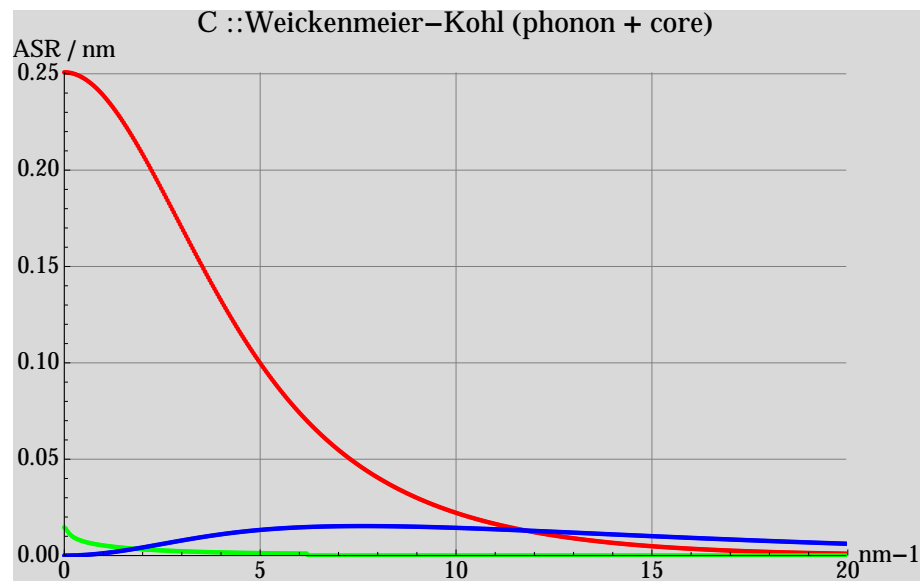


Figure: Carbon. Red: real part, green: imaginary part, blue: thermal diffuse scattering.

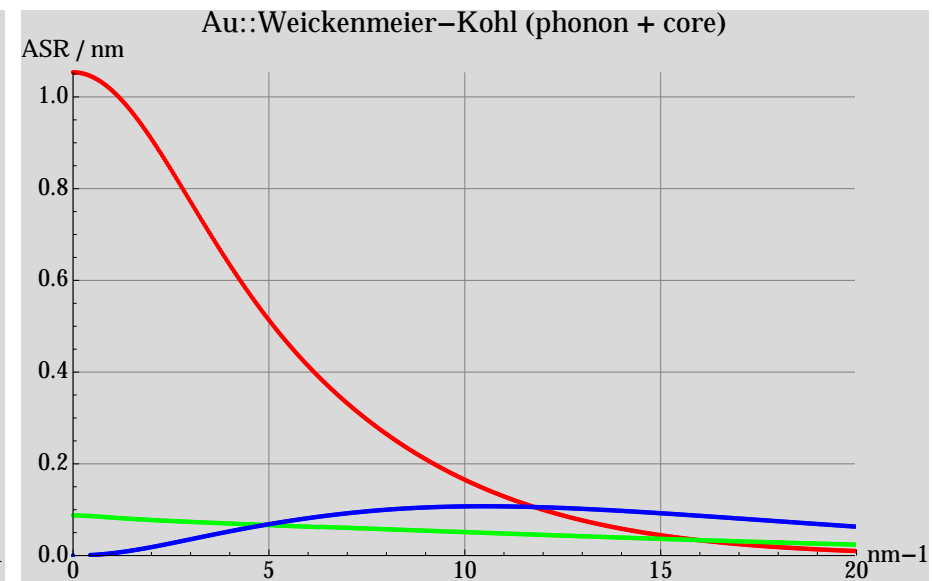


Figure: Gold. Red: real part, green: imaginary part, blue: thermal diffuse scattering.

The TDS (Thermal Diffuse Scattering) at large  $s$  ( $=\sin(\theta)$ ) scales as  $\approx Z^{1.7}$ . It explains HAADF (High Angle Annular Dark Field) atomic column contrast.

# Atomic form factors

Atomic form factors have been tabulated by many authors:

1. Doyle-Turner and Smith-Burge.
2. E.J. Kirkland.
3. Peng-Ren-Dudarev-Whelan.
4. ...

Take care *ASA* of heavy atoms aren't always tabulated properly.

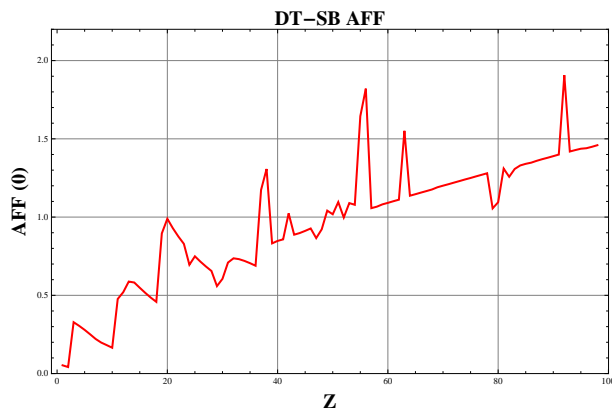


Figure: Doyle-Turner or Smith-Burger.

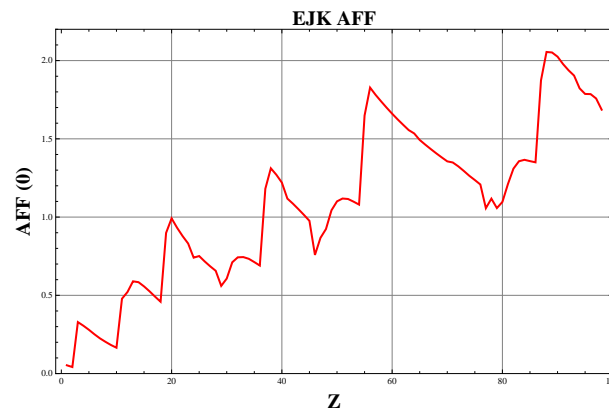


Figure: E. J. Kirkland.

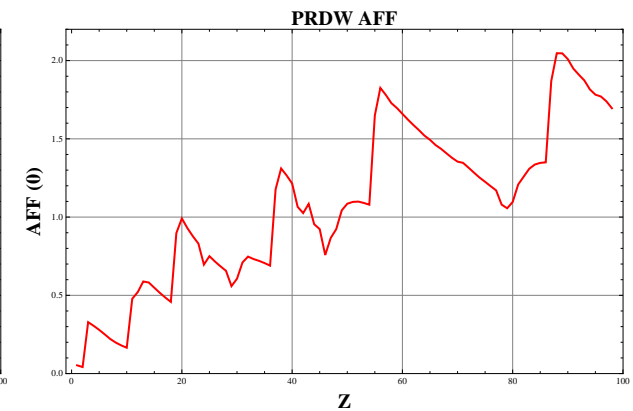


Figure: Peng-Ren-Dudarev-Whelan.

A extremely useful ASA tabulation including phonon and core loss absorption is due to Weickenmeier-Kohl<sup>3</sup>.

<sup>3</sup>A. Weickenmeier, H. Kohl, Acta Cryst. A 47 (1991) 590.

Crystal structure are defined by:

1.  $a, b, c, \alpha, \beta, \gamma$  lattice parameters.
2. Space-group or symmetry operators.
3. Atoms positions (Symbol,  $x, y, z$  with  $0 \leq (x, y, z) < 1$ )

$> 10^5$  crystal structures provided by data bases (ICSD, Min. Soc. Ame., Cryst. Open Database)

Useful servers:

[www.minsocam.org](http://www.minsocam.org)

[www.crystallography.net](http://www.crystallography.net)

[www.cryst.ehu.es](http://www.cryst.ehu.es)

# ICSD & AMS: data bases for crystal structures

Available CIF files

<input checked="" type="radio"/> Triiron tetraoxide	<input type="radio"/> Iron oxide
<input type="radio"/> Iron oxide (0.93/1)	<input type="radio"/> Triiron tetraoxide
<input type="radio"/> Iron oxide	<input type="radio"/> Iron oxide (0.93/1)
<input type="radio"/> Iron(III) oxide - alpha	<input type="radio"/> Iron(III) oxide - alpha
<input type="radio"/> Iron(III) oxide - alpha	<input type="radio"/> Iron(III) oxide - alpha
<input type="radio"/> Iron(III) oxide - alpha	<input type="radio"/> Iron(III) oxide - alpha
<input type="radio"/> Iron(III) oxide - alpha	<input type="radio"/> Iron oxide (2.93/4)
<input type="radio"/> Iron oxide (2.93/4)	<input type="radio"/> Iron oxide (2.95/4)
<input type="radio"/> Iron oxide (2.94/4)	<input type="radio"/> Iron oxide (2.93/4)
<input type="radio"/> Iron oxide (2.95/4)	<input type="radio"/> Iron oxide (2.94/4)
<input type="radio"/> Iron oxide (2.94/4)	<input type="radio"/> Iron oxide (2.93/4)
<input type="radio"/> Iron oxide (2.94/4)	<input type="radio"/> Iron oxide (2.94/4)
<input type="radio"/> Iron oxide (2.96/4)	<input type="radio"/> Iron oxide (2.96/4)
<input type="radio"/> Iron oxide (2.96/4)	<input type="radio"/> Iron oxide (2.96/4)
<input type="radio"/> Iron oxide (2.94/4)	<input type="radio"/> Iron oxide (2.95/4)
<input type="radio"/> Iron(III) oxide - alpha	<input type="radio"/> Iron oxide (21.34/32) - gamma
<input type="radio"/> Iron oxide (21.34/32) - gamma	<input type="radio"/> Iron(III) oxide - alpha
<input type="radio"/> Iron diiron(III) oxide	<input type="radio"/> Iron(III) oxide - alpha
<input type="radio"/> Iron oxide (.92/1)	<input type="radio"/> Iron oxide (.92/1)
<input type="radio"/> Iron oxide (.93/1)	<input type="radio"/> Iron oxide (.88/1)
<input type="radio"/> Iron oxide (.89/1)	<input type="radio"/> Iron oxide (.9/1)
<input type="radio"/> Iron oxide (.91/1)	<input type="radio"/> Iron oxide (.92/1)
<input type="radio"/> Iron oxide (0.95/1)	<input type="radio"/> Iron oxide (0.95/1)
<input type="radio"/> Iron(III) oxide - alpha	<input type="radio"/> Diiron(III) oxide - alpha

Fe (O) at : (0.375, 0.375, 0.875)

ICSD\_82237 : [0, 0, 1]

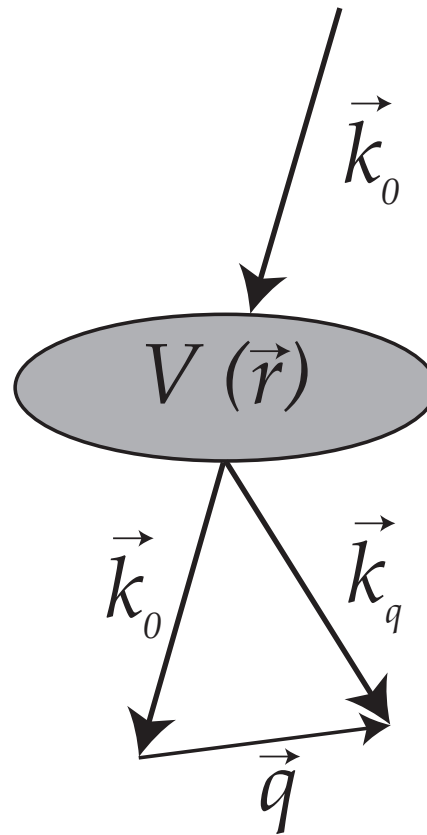
Projections

[0, 0, 1]     [1, 0, 0]     [0, 1, 0]

Cancel    Select

# Scattering & diffraction

# Scattering: electron-matter interaction



An incident electron of wave vector  $\vec{k}_0$  interacts with a solid of scalar potential  $V(\vec{r})$ . The wave vector of the scattered electron is  $\vec{k}_q = \vec{k}_0 + \vec{q}$  where  $\vec{q}$  is the momentum transferred by the solid<sup>4</sup>.

Elastic scattering  $\longrightarrow ||\vec{k}_q|| = ||\vec{k}_0||$ .

<sup>4</sup>Magnetic and spin effects are ignored.

With energy conservation and momentum transfer ( $\vec{s}_g = 0$ ), i.e. elastic scattering:

$$|\vec{k}_i + \vec{g}| = |\vec{k}_g|$$

$$k_i^2 + 2 \times k_i \times g \times \cos(\vec{k}_i, \vec{g}) + g^2 = k_g^2$$

$$2k_i \times \cos(\vec{k}_i, \vec{g}) = -g$$

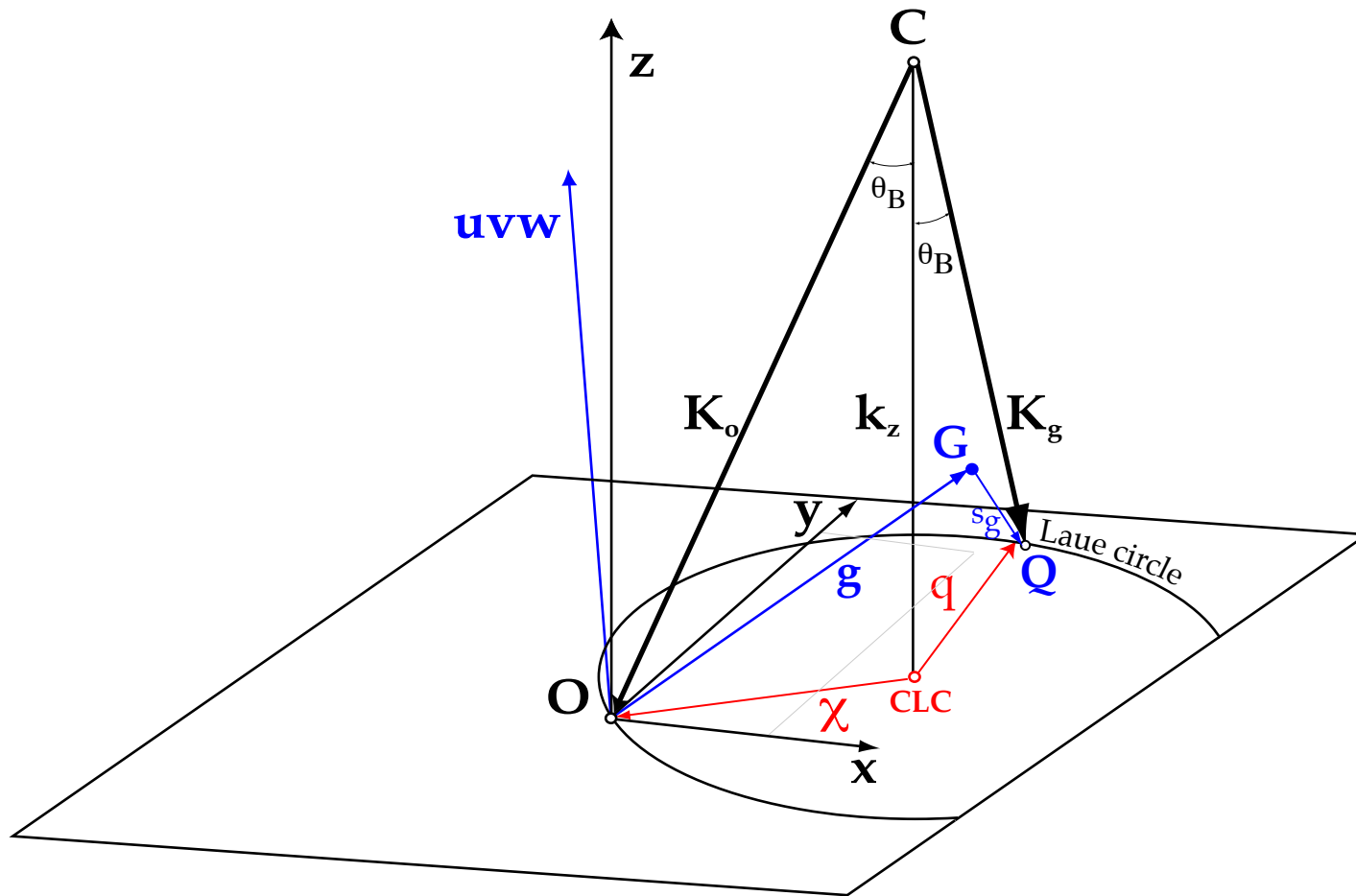
$$2k_i \times \cos(90^\circ - \theta_B) = -g$$

$$\frac{2}{\lambda} \times \sin(\theta_B) = g = \frac{1}{d_g}$$

$\implies$  Bragg law:

$$2 \times d_{hkl} \times \sin(\theta_B) = \lambda$$

# Diffraction geometry: small angle approximation



Center of the Ewald sphere ( $C$ ) and Center of the Laue Circle ( $CLC$ ), projection of  $C$  onto the zero order Laue zone. All reflections on the circle of radius  $\chi$  are at exact Bragg condition. Notice that the Bragg angles are **pretty small** (of the order a few  $^\circ$ ) and that consequently the **small angle approximation** is quite good.



The structure factor gives the scattering *strength* of (h,k,l) planes.

$$F_{hkl} = \sum_{i=\text{atomes}} f_i(s_{hkl}) e^{(2\pi i(hx_i + ky_i + lz_i))}$$

where:

1.  $f_i(s_{hkl})$  is the atomic scattering amplitude.
2.  $(x_i, y_i, z_i)$  are the fractional coordinates of atom  $i$  ( $0 \leq x_i < 1$ ).
3.  $s_{hkl} = \frac{\sin(\theta_B)}{\lambda} = \frac{1}{2d_{hkl}}$ .

In general all reflections allowed by the Bravais lattice are visible:

**Simple cubic:**  $(hkl)$  no condition.

1 atom at  $(0, 0, 0)$ .

$$\implies F_{hkl} = f_i(s_{hkl})$$

**Body centered cubic:**  $(hkl) : h + k + l = 2n$

2 atoms at  $(0,0,0)$  and  $(\frac{1}{2}, \frac{1}{2}, \frac{1}{2})$ .

$$\implies F_{hkl} = f_i(s_{hkl}) \left[ 1 + e^{\pi i(h+k+l)} \right]$$

**Face centered cubic:**  $(hkl)$  all even or odd.

4 atoms at  $(0, 0, 0)$ ,  $(0, \frac{1}{2}, \frac{1}{2})$ ,  $(\frac{1}{2}, 0, \frac{1}{2})$ ,  $(\frac{1}{2}, \frac{1}{2}, 0)$

$$\implies F_{hkl} = f_i(s_{hkl}) \left[ 1 + e^{\pi i(h+k)} + e^{\pi i(h+l)} + e^{\pi i(k+l)} \right]$$

# Kinematical diffraction: $\langle q|U(z,0)|\chi \rangle$

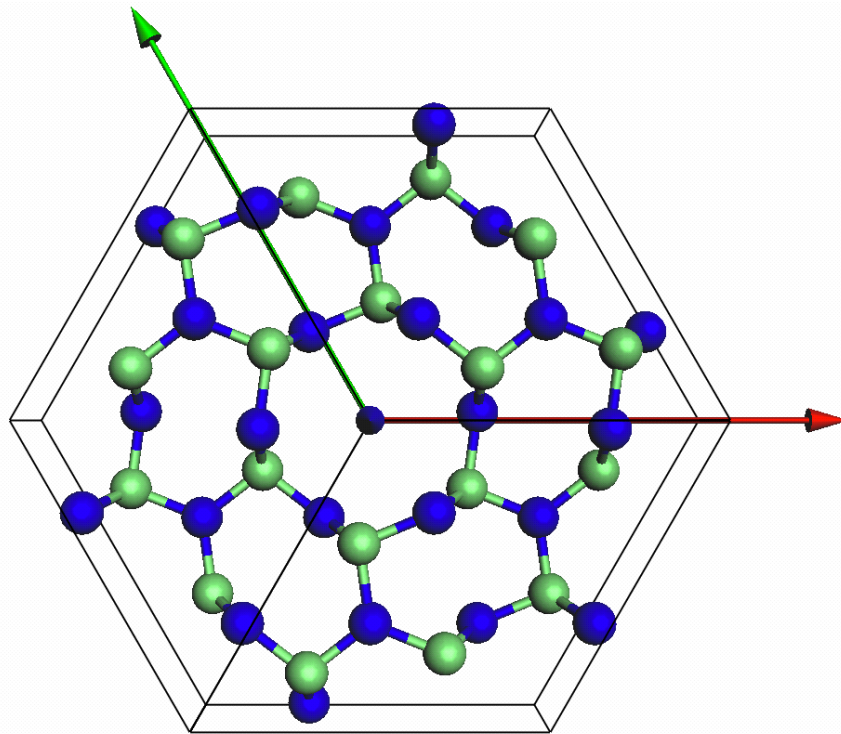


Figure: Model ( $Ge_3N_4$ ).

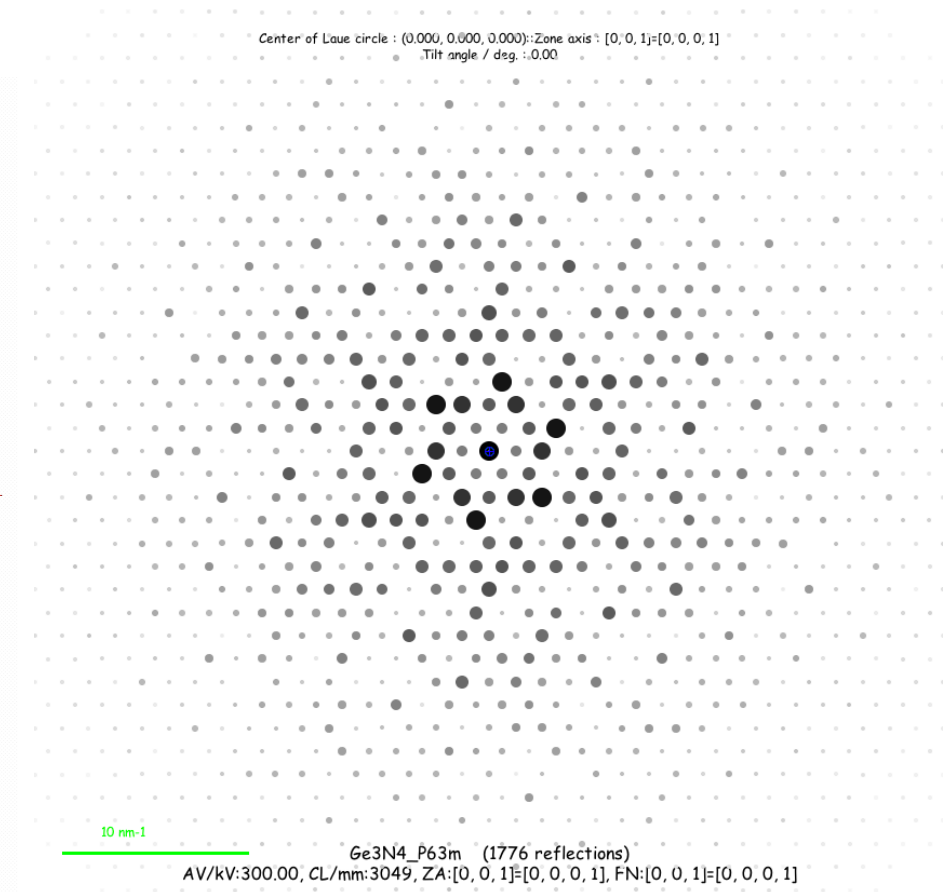


Figure: Kinematical diffraction  $Ge_3N_4$ , [001].

$\langle q|U(z,0)|\chi\rangle \implies$  Fourier transform of object wavefunction

Dynamical scattering (many approaches under small angle approximation and elastic scattering).

Including inelastic scattering more complicated and computer intensive.

# Gratias & Portier: small angle & elastic scattering approximations

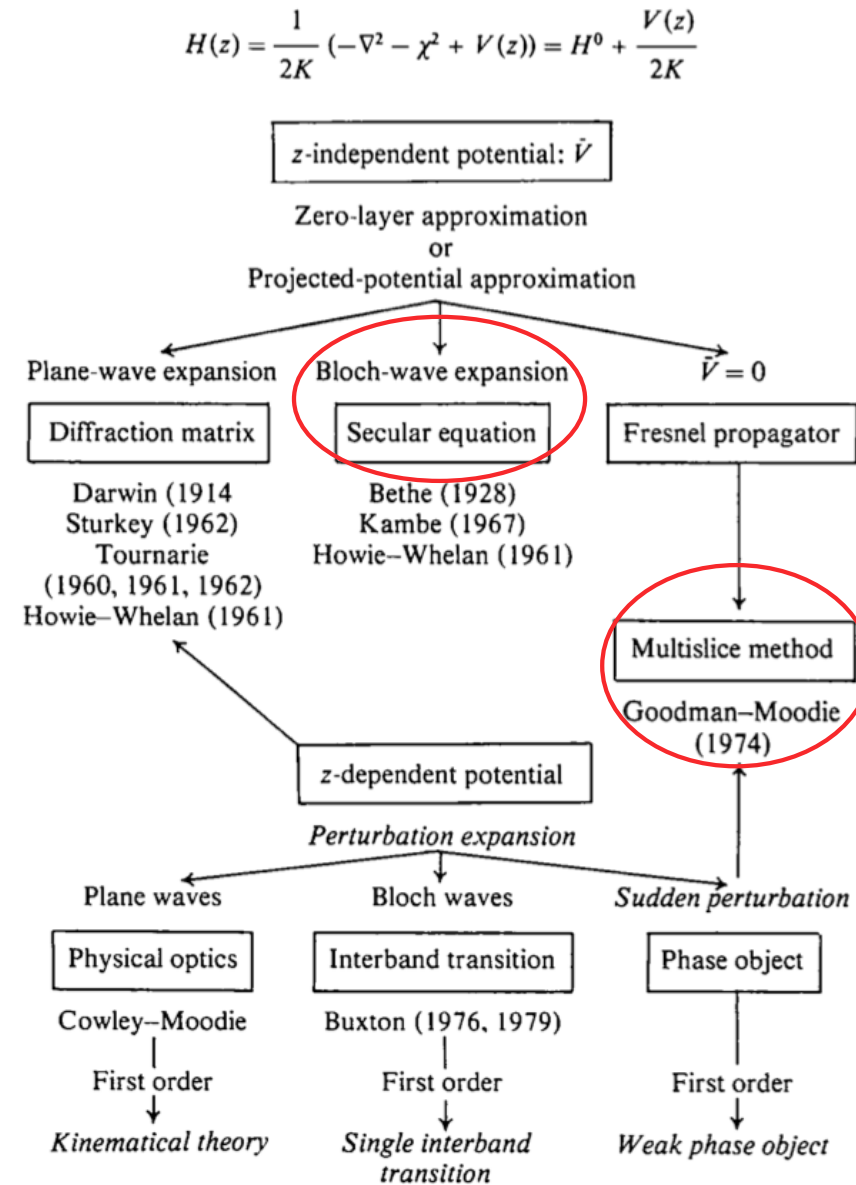


Figure: From Gratias and Portier<sup>5</sup>

<sup>5</sup>D. Gratias and R. Portier, Acta Cryst. **A39** (1983) 576.

# The two most employed calculation methods

All approximations are numerically equivalent, but perform best in particular cases.

We will consider only 2 approximations:

- ▶ The multislice approximation<sup>6</sup>.
- ▶ The Bloch-wave method<sup>7</sup>.

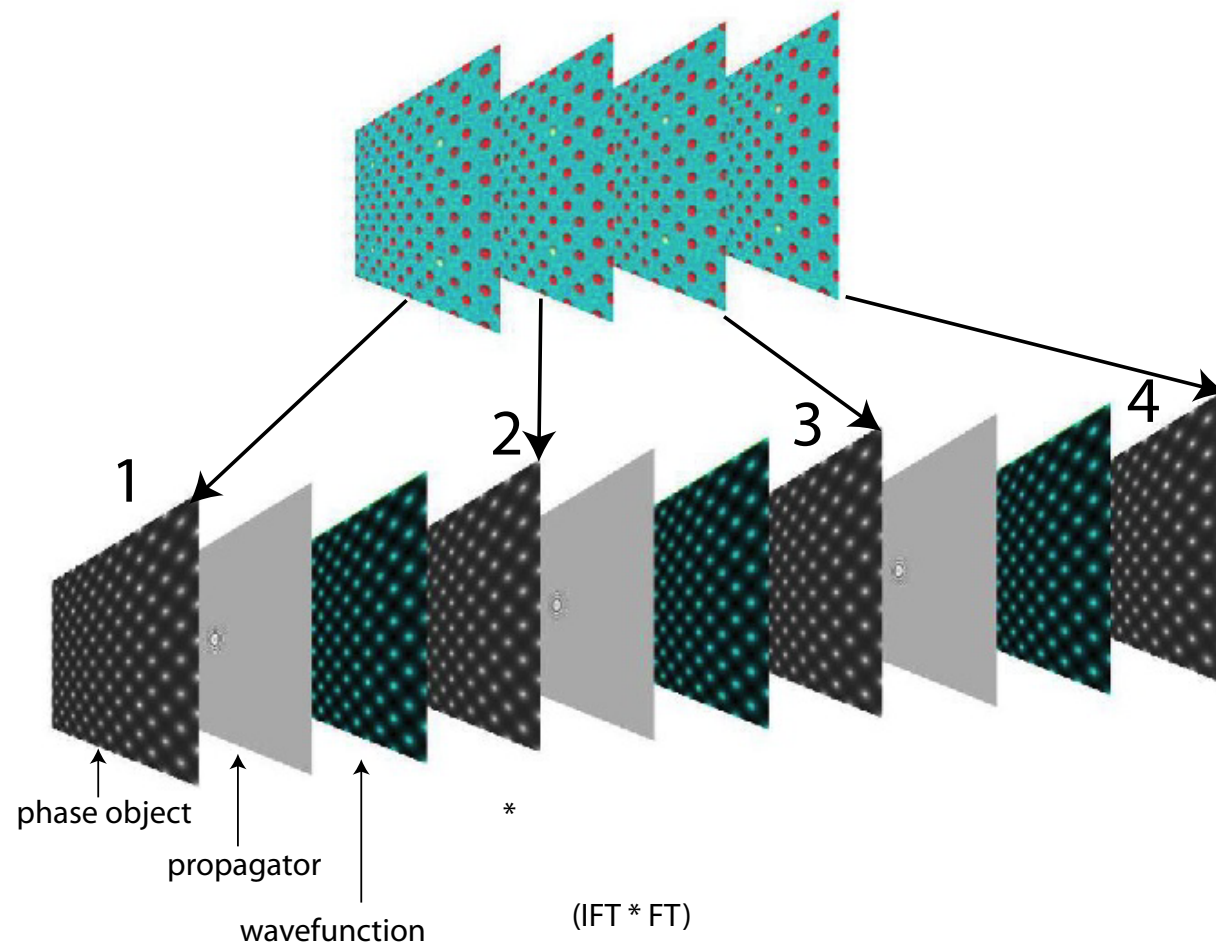
The multislice method performs best when simulating crystalline or amorphous solids of large unit cell or containing defects while the Bloch-wave method is adapted to the calculation of crystalline solids of small unit cell and in any  $[uvw]$  orientation. The Bloch-wave method has also several advantages (speed, ease of use) for simulating CBED, LACBED or PED patterns and for polarity and chirality determination.

---

<sup>6</sup>J. Cowley and A.F. Moodie, Proc. Phys. Soc. B70 (1957) 486, 497 and 505.

<sup>7</sup>H. A. Bethe, Ann. Phys. 87 (1928), 55.

# Multislice method



The solid is sliced into thin sub-slices. The incident wave-function is transferred by the first slice (diffraction) and propagated to the next one. The propagation is done within the Fresnel approximation, the distance between the slices being 20 - 50 times the wavelength<sup>8</sup>.

$$\Psi(i + 1) = [\Psi(i)PO(i)] \otimes FP_{i \rightarrow i+1}$$

<sup>8</sup><file:///localhost/Applications/jemsMacOSX/html/PtOct/a.html>

Can simulate:

- ▶ Perfects crystals.
- ▶ Defects under the periodic continuation assumption <sup>9</sup>.

2 steps:

- ▶ Diffractor: transfer by a slice  $\Rightarrow$  multiplication by phase object function ( $POF(\vec{\rho})$ ).
- ▶ Propagator: propagation between slices  $\Rightarrow$  convolution by the Fresnel propagator (is nowadays performed by a FFT followed by a multiplication and an inverse FFT ( $FT^{-1}$ , multiplication, FFT)).

---

<sup>9</sup><file:///localhost/Applications/jemsMacOSX/html/PtOct/b.html>

<sup>10</sup>K. Ishizuka, Acta Cryst. A33 (1977) 740-749.



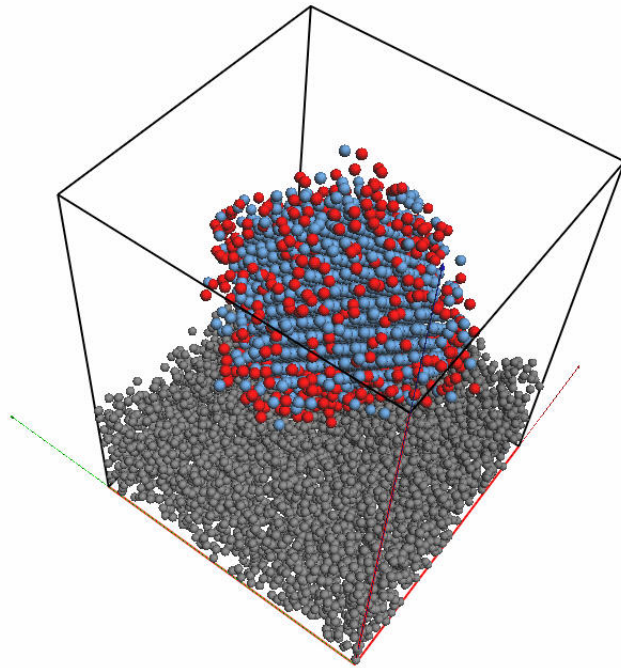


Figure: Model (one unit cell).

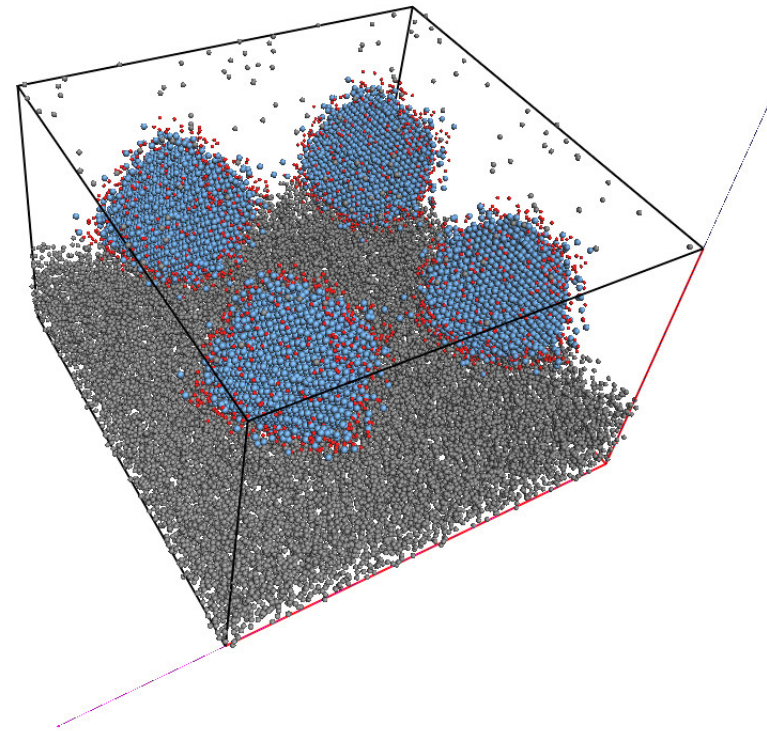
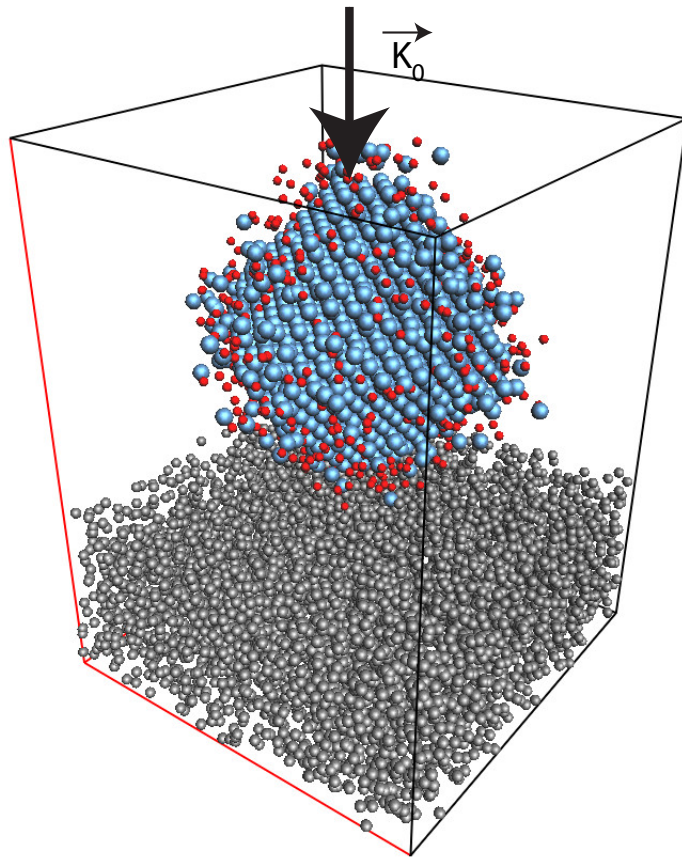


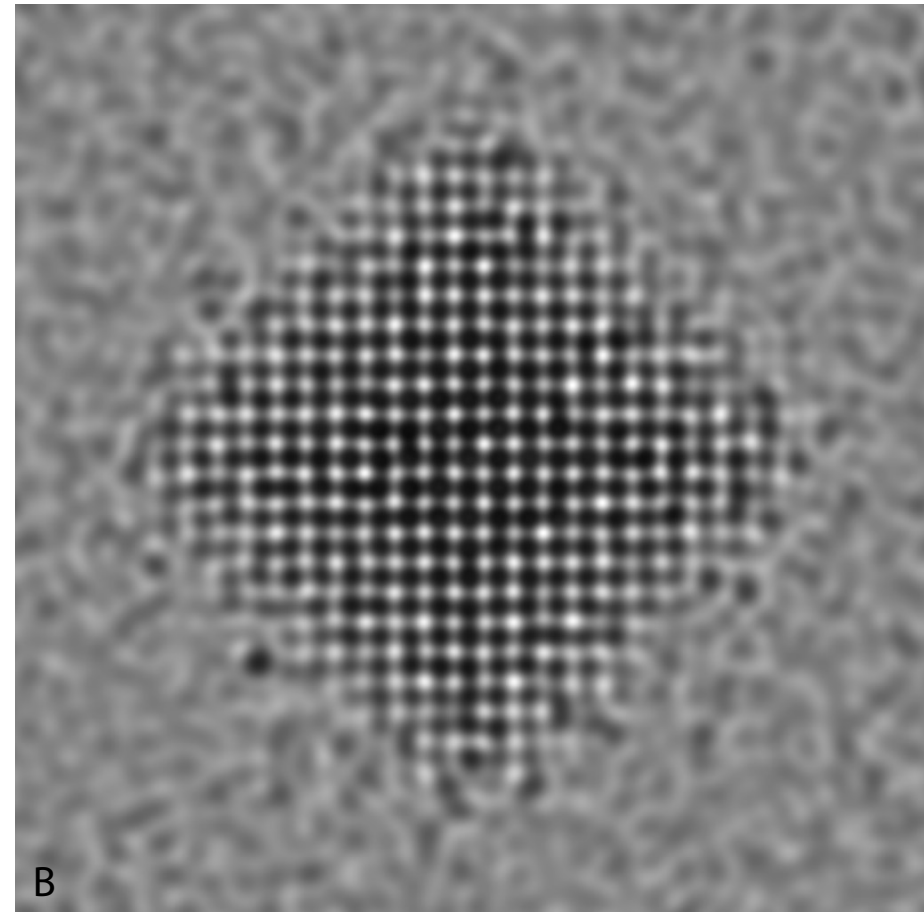
Figure: Model with periodic continuation (2 x 2 unit cells).

<sup>11</sup>A.J. Skarnulis, Thesis, Arizona State University 1975.

# Example multislice: Pt catalyst



A



B

A: catalyst model (9500 atoms)<sup>12</sup>. B: HREM image (Jeol 400kV).

# Bloch wave method: z-independent potential

When the scattering potential is periodic, the eigenstates  $|j\rangle$  of the propagating electrons are Bloch waves. The hamiltonian of the system is projected on the eigenstates  $|j\rangle$  with eigenvalues  $\gamma_j$  ("anpassung" parameter).

$$\hat{H} = \sum_j \gamma_j |j\rangle \langle j|$$

The evolution operator is then given by (since  $V = V(\vec{\rho})$ ):

$$\hat{U}(z, 0) = e^{-i\hat{H}z} = \sum_j e^{-i\gamma_j z} |j\rangle \langle j|$$

The wave-function at z developed on plane waves basis  $|q\rangle$ :

$$\Psi(z) = \sum_q \phi_q(z) |q\rangle$$

$$\phi_q(z) = \langle q | \hat{U}(z, 0) | 0 \rangle = \sum_j e^{-i\gamma_j z} \langle q | j \rangle \langle j | 0 \rangle$$

$$c_0^{*j} = \langle j | 0 \rangle \quad \text{and} \quad c_q^j = \langle q | j \rangle$$

where in usual notation  $c_0^{*j}$  and  $c_q^j$  are the Bloch-wave excitations (component of the initial state  $|0\rangle$  on  $|j\rangle$ ) and coefficients (component of reflection  $|q\rangle$  on  $|j\rangle$ ) respectively.

Simulation of:

- ▶ SAED (kinematical and dynamical).
- ▶ CBED (polarity).
- ▶ LACBED (specimen thickness, symmetry).
- ▶ PED (Precession Electron Diffraction).
- ▶ HRTEM.

Works best for small lattice parameters crystals<sup>13</sup>.

---

<sup>13</sup>Some more details in Appendix1.

# CBED: ZnTe [110]

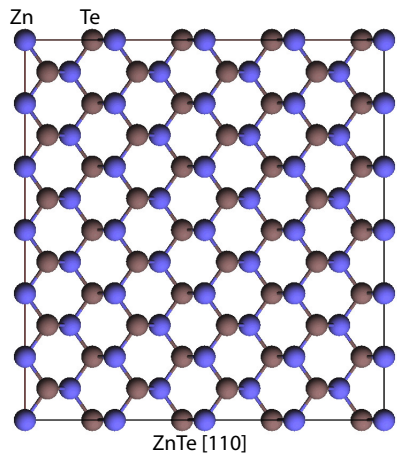


Figure: ZnTe [110].

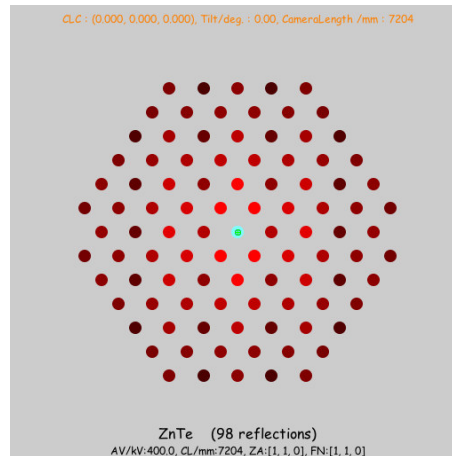


Figure: Reflections (1 + 49),  $|\chi| \geq 0$ .

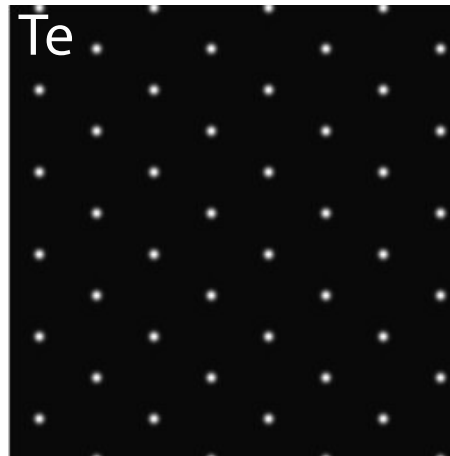


Figure: Bloch-wave 1 (Te 1s).

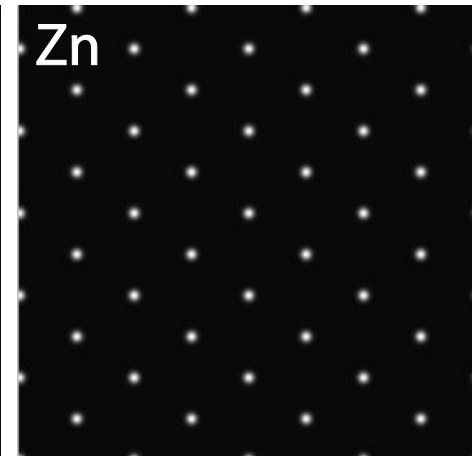


Figure: Bloch-wave 2 (Zn 1s).

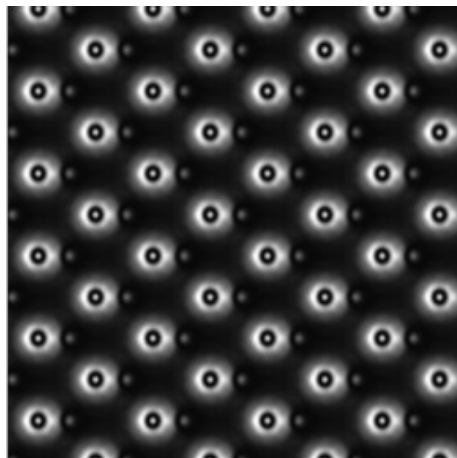


Figure: Bloch-wave 5 (Te-Zn).

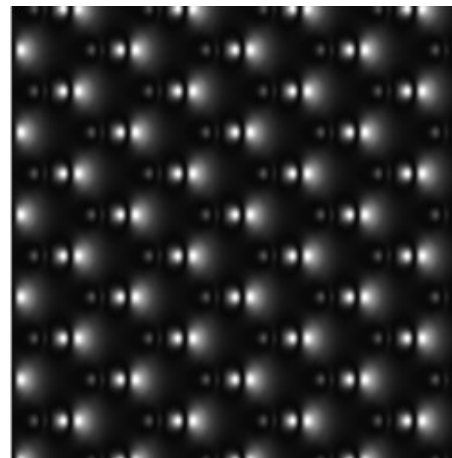


Figure: Bloch-wave 7 (Te-Zn).

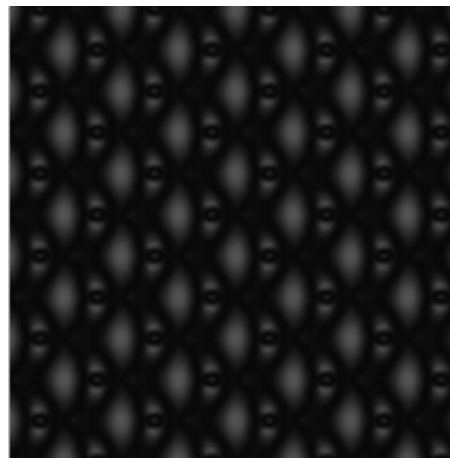


Figure: Bloch-wave 8 (Te-Zn).

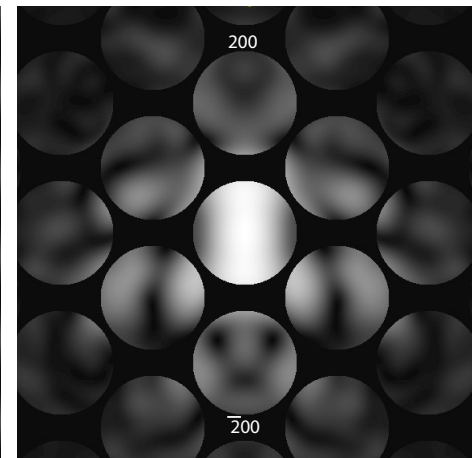
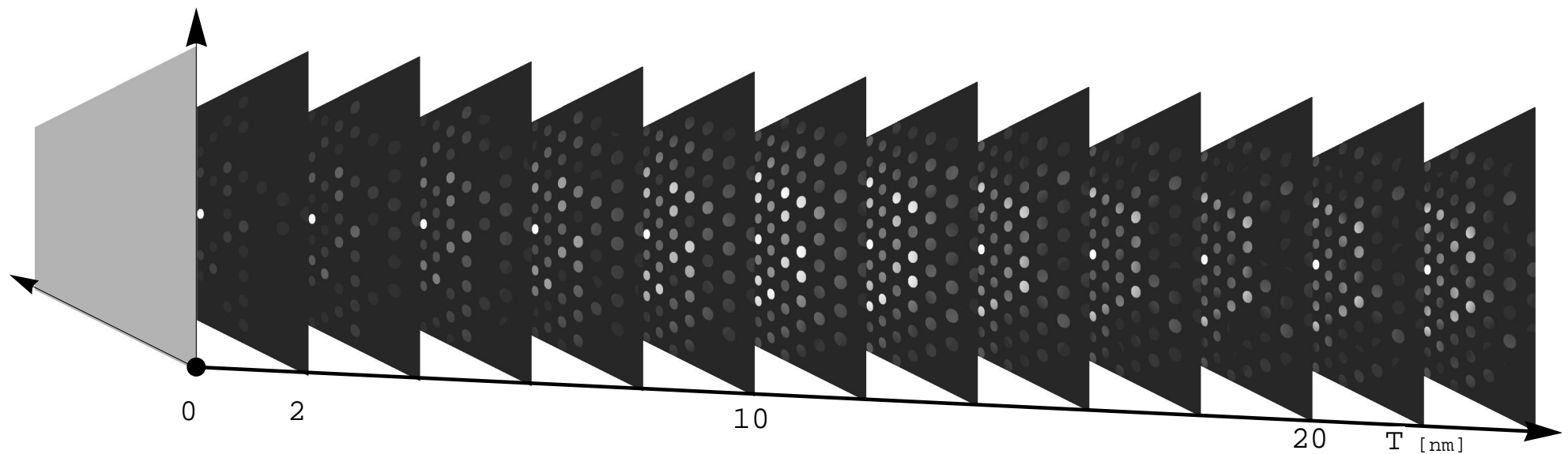


Figure: CBED (ZnTe polarity).



In BFP diffraction pattern depends specimen thickness.

Goodness of dynamical diffraction theories?

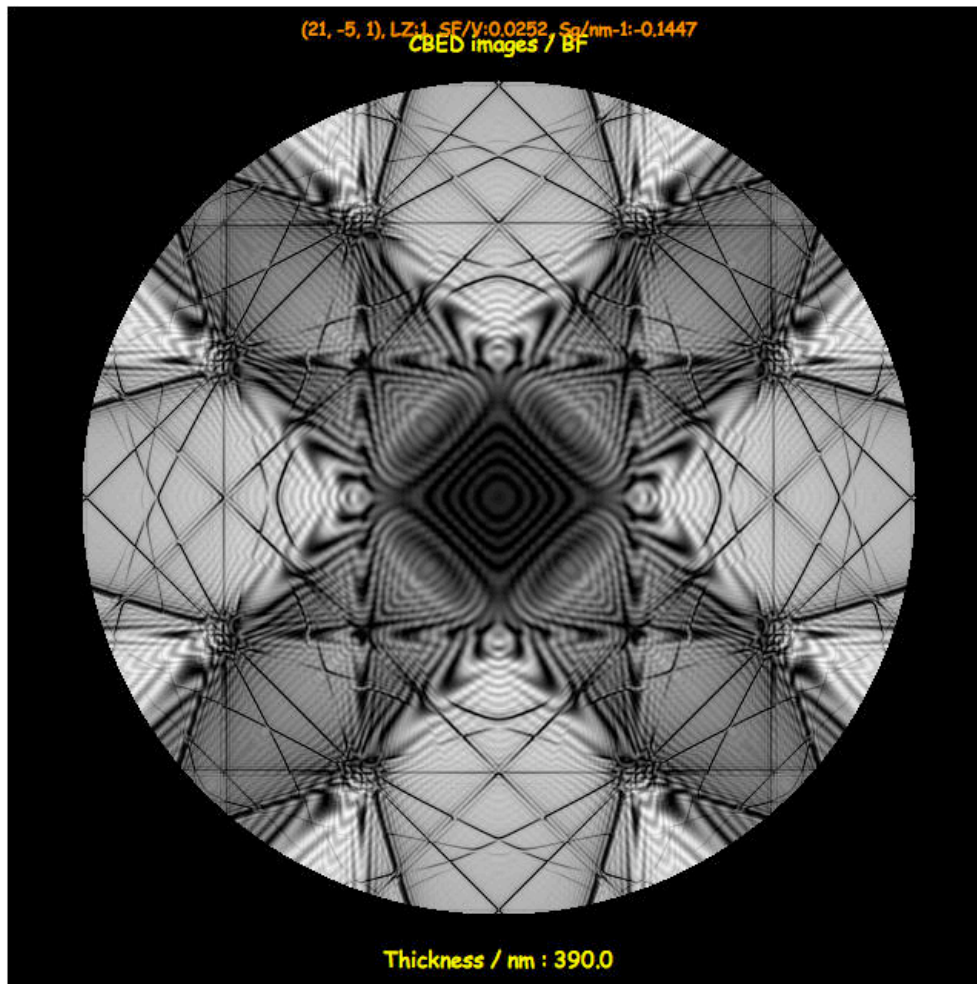


Figure: LACBED Si [001]: simulation.

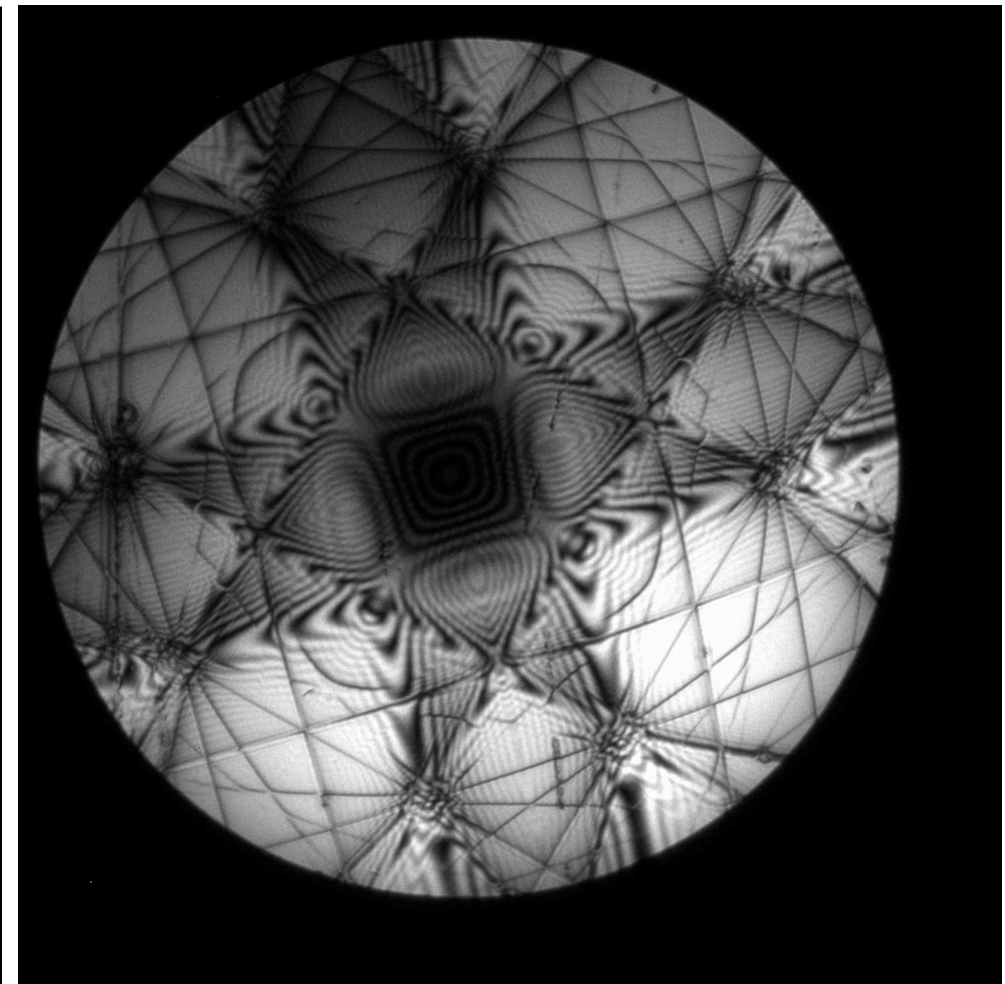


Figure: LACBED Si [001]: experimental (Web site EM centre - Monash university, J. Etheridge).

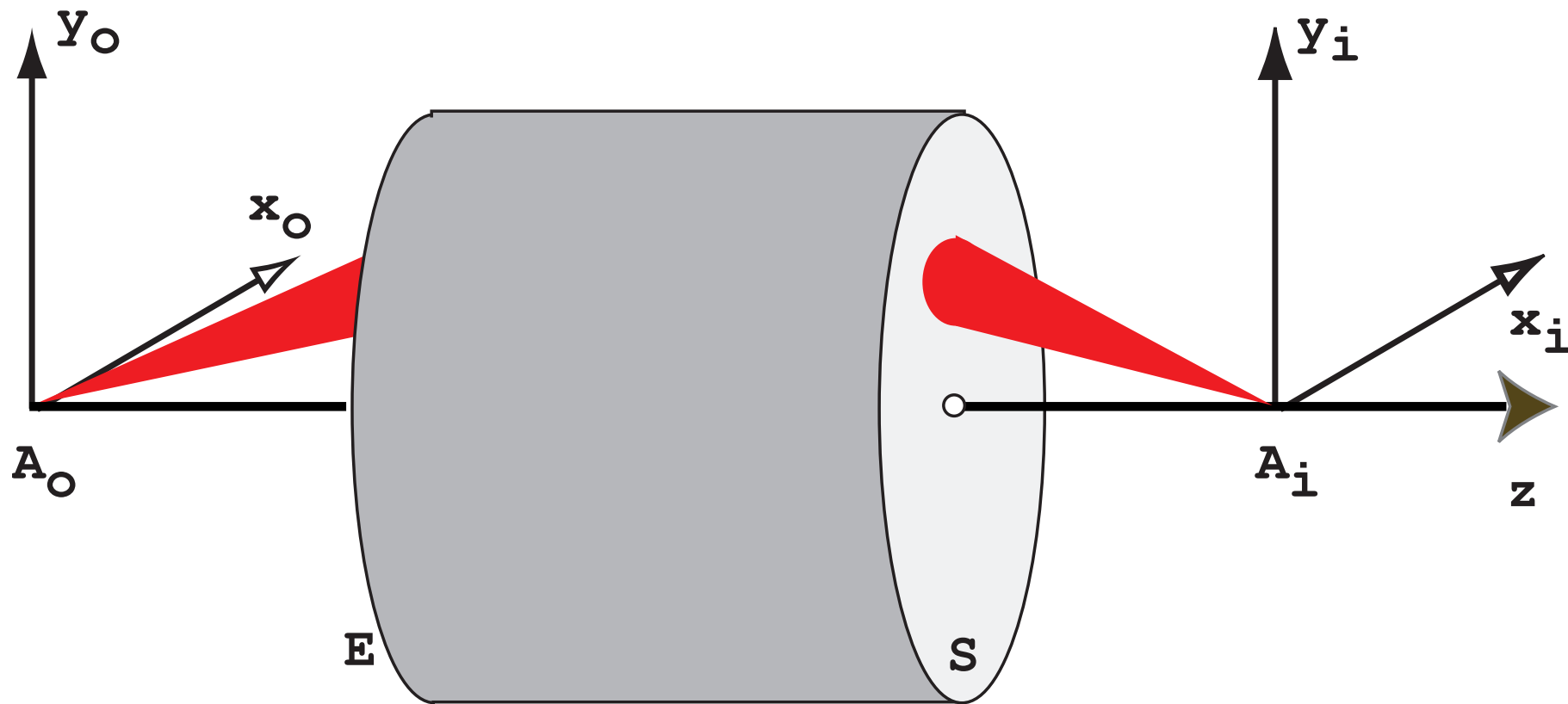
Note that the experimental LACBED pattern is blurred (inelastic scattering and/or MTF of CCD camera?).

# Image formation

- ▶ Abbe image formation.
- ▶ Transfer function.
- ▶ Perfect thin lens.
- ▶ Aberrations.



# Optical system



An optical system produces the **image**  $A_i$  of a **point source** object  $A_o$ .  $A_o$  and  $A_i$  are said to be conjugate.  $A_i$  is **not** a point since any optical system is diffraction limited. This limitation is introduced by the entrance and exit pupils of the optical system.

Some light rays emitted by object point  $A_o$  do not reach the image at point  $A_i$ .

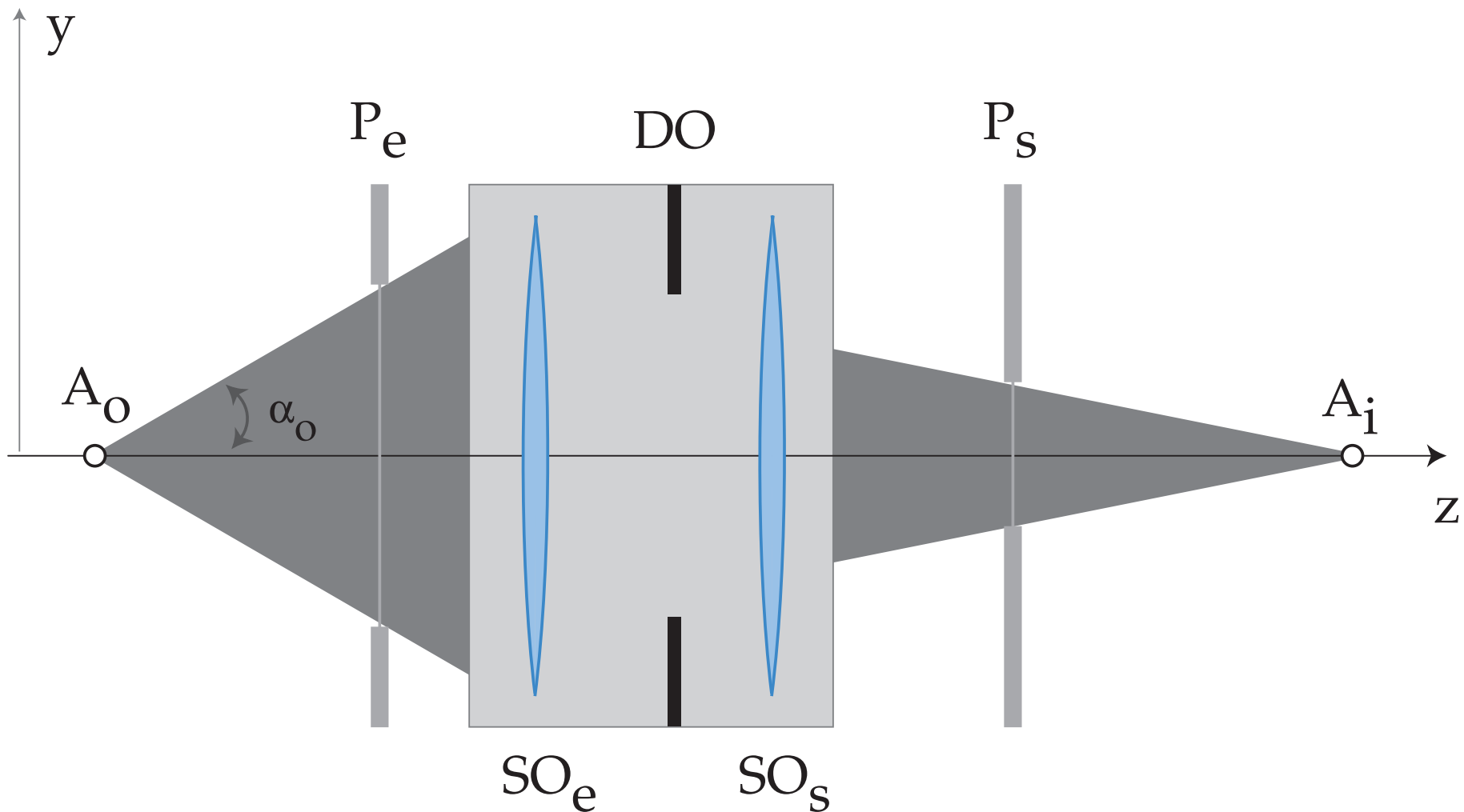
Position of  $A_i$   $\longrightarrow$  intersection of the reference light ray (non deviated) and the image plane.

The image of a point source is a **spot** whose shape and intensity depend of the quality of the optical system.

Two types of aberrations:

1. **Monochromatic.**
2. Chromatic ( $\lambda$  dependent).

# Pupils



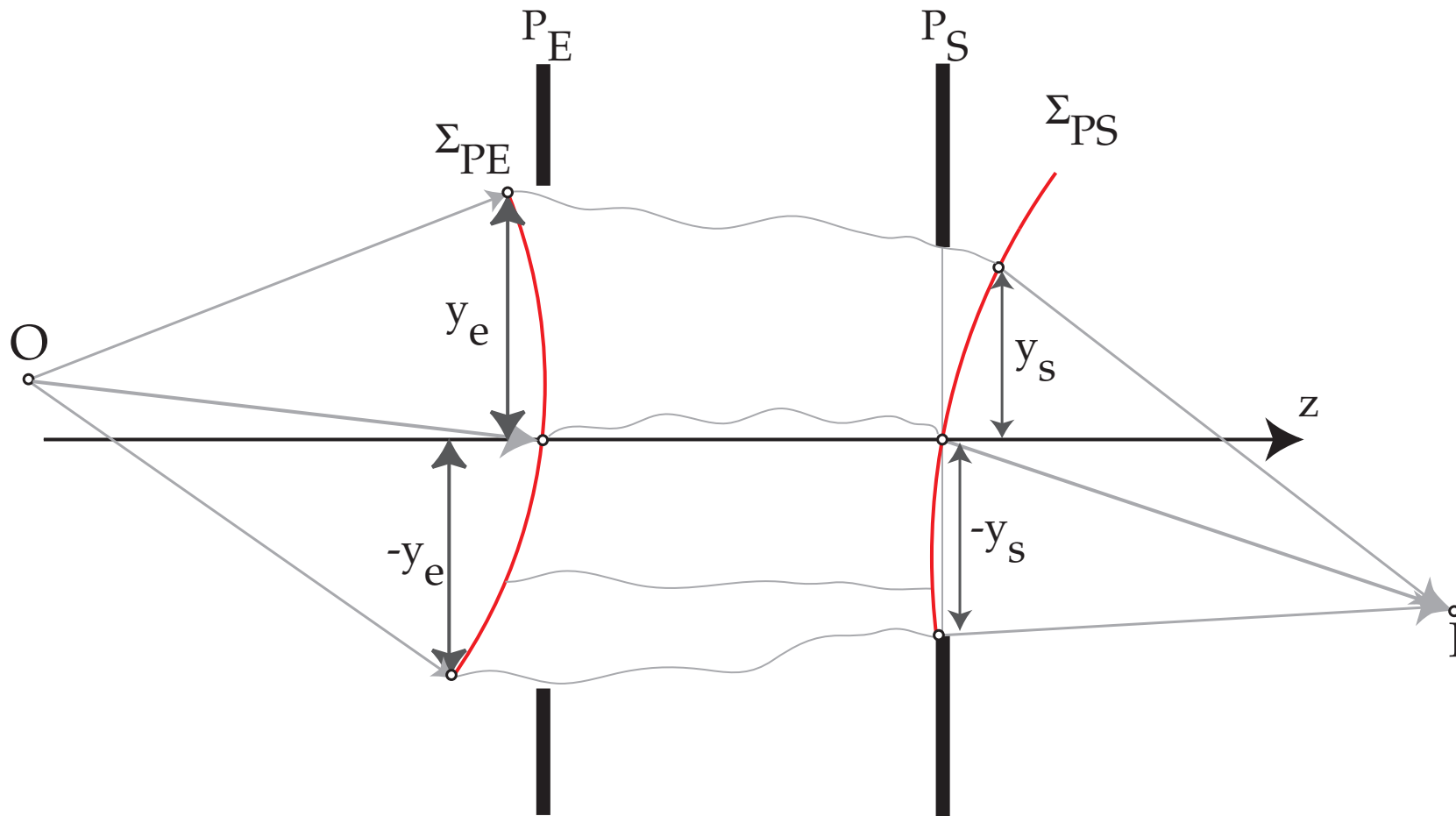
Any optical system can be characterised by an entrance pupil  $P_e$  and an exit pupil  $P_s$ . The pupils are the image of the opening aperture  $DO$  by the entrance and exit optical subsystems  $SO_e$  and  $SO_s$ . What are  $P_e$  and  $P_s$  for a thin lens?

In order to evaluate the monochromatic aberrations one must define a function characteristic of the optical system.

This function will depend on:

1. The selected reference planes.
2. The optical path followed by the light ray.

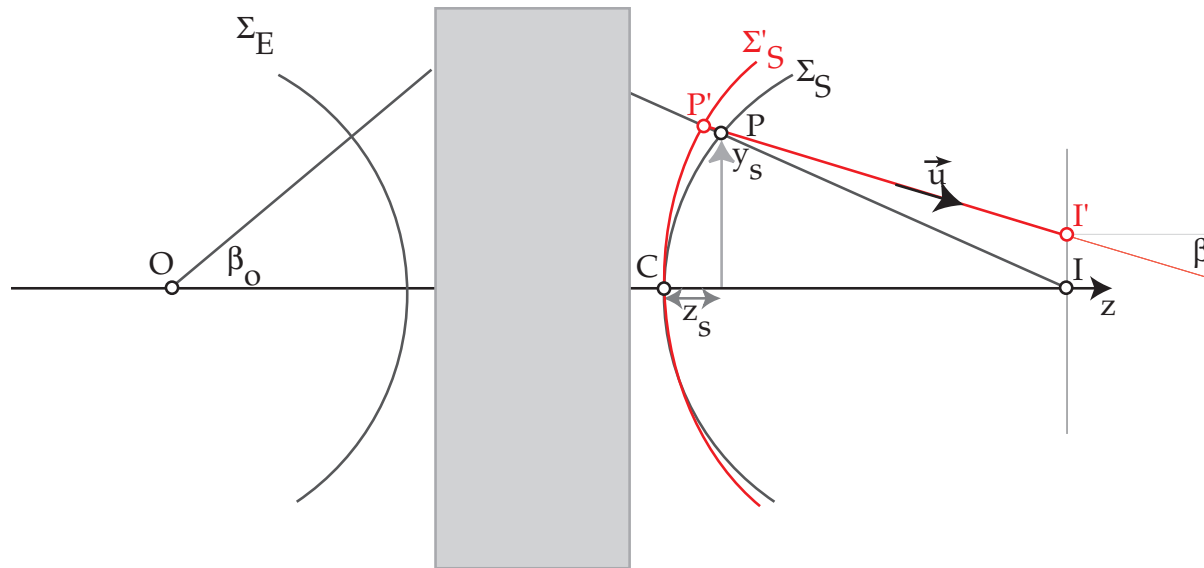
# Optical Path Length: OPL



- ▶ **Before**  $P_E$  the reference wavefront  $\Sigma_{PE}$  is spherical (point source at  $O$ ).
- ▶ **After**  $P_S$  the reference wavefront  $\Sigma_{PS}$  is spherical (converges towards  $I$ ).

For a perfect optical system, both the entrance  $\Sigma_{PE}$  and exit  $\Sigma_{PS}$  wavefronts are spherical. The **O**ptical **P**ath **L**ength from  $O$  to  $I$  is independent of the path.

# Optical Path Difference (OPD): aberrations



In the presence of aberrations the wavefront  $\Sigma'_S$  is no more spherical. The **O**ptical **P**ath **D**ifference (distance between the deformed  $\Sigma'_S$  and spherical wavefront  $\Sigma_S$ ) introduces a **phase shift**  $\delta\phi$ . With  $P'$  close to  $P = (x_s, y_s)$  on reference sphere  $\Sigma_S$ , the OPD at  $P' =$  (i.e. OPL from  $P'$  to  $P$ ) is given by (Fermat principle):

$$W(x_s, y_s) = n_i \overline{P'P}$$

$n_i$  refractive index of the medium  $\longrightarrow$  phase shift:

$$\delta\phi = e^{2\pi i \frac{W(x_s, y_s)}{\lambda}}$$

# Transverse geometric aberrations: $\vec{\epsilon}$

The transverse geometric aberrations are proportional to  $\frac{d}{d\theta}$  wavefront aberrations<sup>14</sup>:

$$\epsilon_x = -\frac{f \partial W}{n_i \partial x_s}$$
$$\epsilon_y = -\frac{f \partial W}{n_i \partial y_s}$$

$f$  focal length.

The OPD's introduced by all the aberrations of the imaging system are collected in a function  $\chi(\vec{u})$  and the phase shift is<sup>15</sup>:

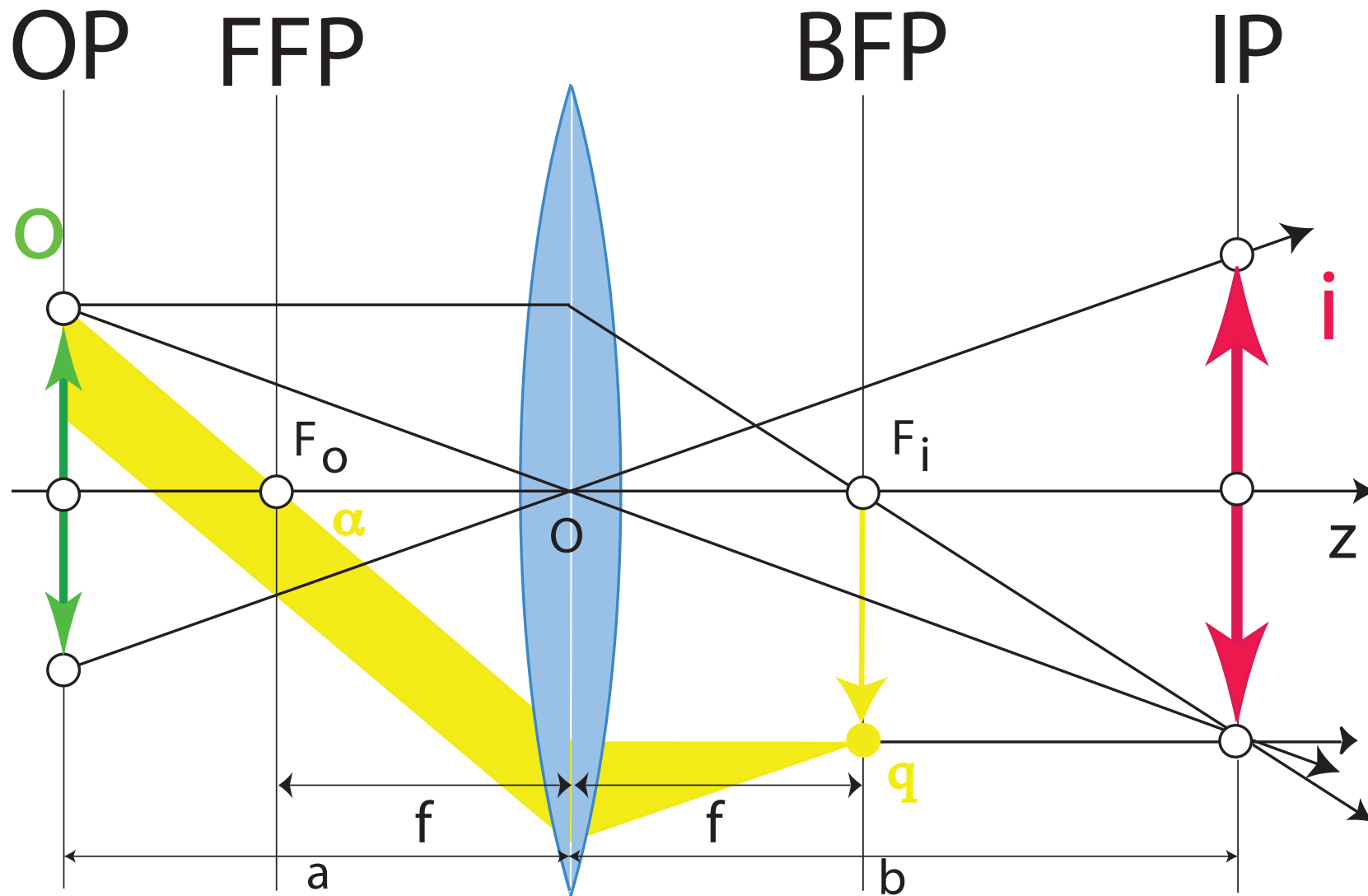
$$\tilde{T}(\vec{u}) = e^{i\chi(\vec{u})}$$

$\tilde{T}(\vec{u})$  has been first employed by Abbe in his description of image formation (1866).

<sup>14</sup> $P(x_s, y_s)$  on the spherical reference wavefront can be characterised by the radial angle  $\theta$ .

<sup>15</sup>The angle  $\theta$  corresponds (through Bragg law) to a spatial frequency  $\vec{u}$ , i.e. a distance in the back focal plane.

# Paraxial optics: principal rays



Principal rays of paraxial optics. Reflection (plane wave) making an angle  $\alpha$ , where  $\alpha = 2\theta_B$ , corresponds to spatial frequency  $u$ .



# Microscope modelling: Abbe image formation theory

Objective lens is modelled as a thin lens that brings Fraunhofer diffraction pattern at finite distance (i.e. in its **Back Focal Plane**).

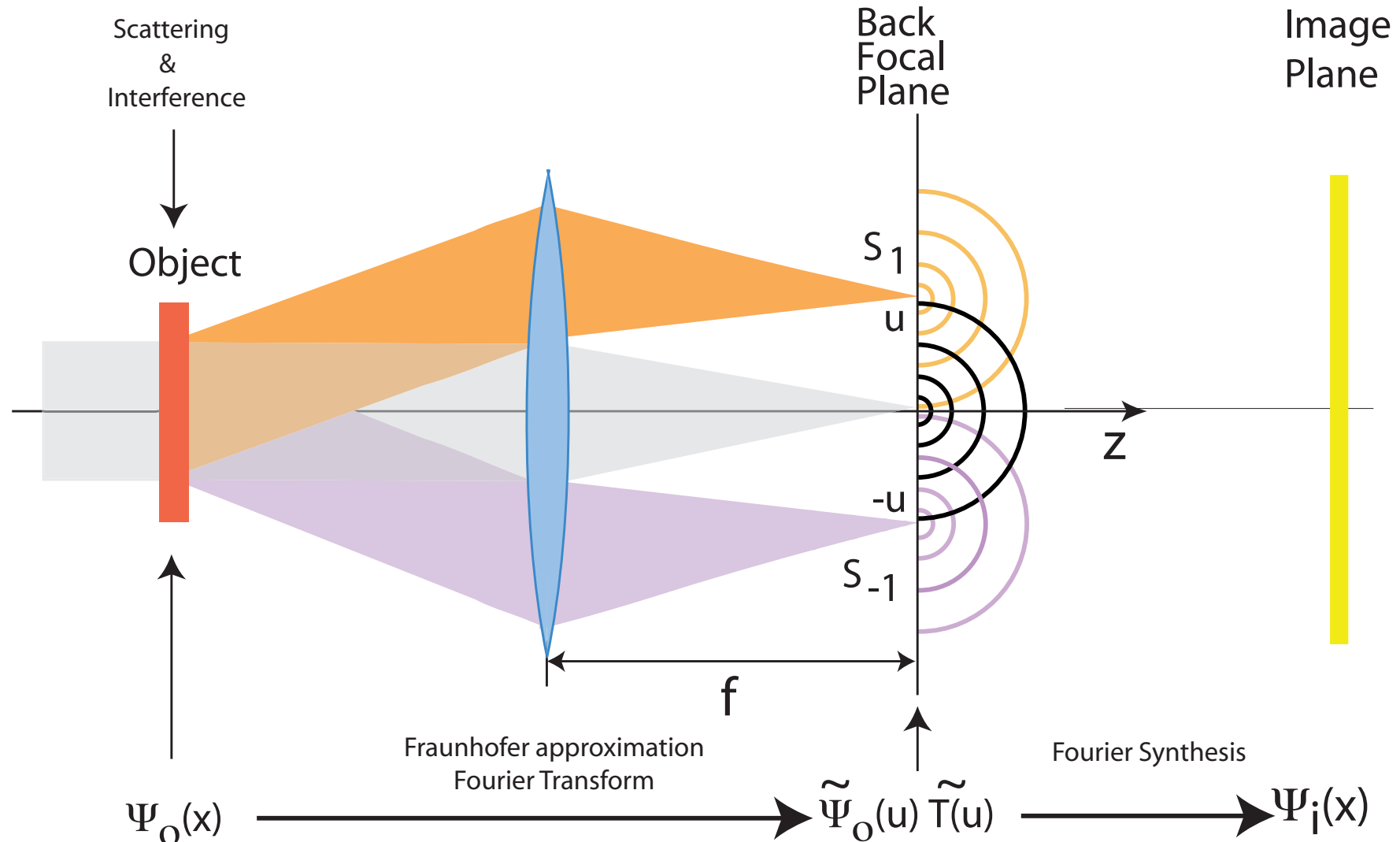


Image forming system has 2 properties (**Abbe theory**):

- ▶ Linear.
- ▶ Space invariant.

**Coherence** of illumination:

- ▶ Source size (spatial coherence).
- ▶ Energy spread (temporal coherence).

Partial coherence (always the case):  $\tilde{T}(q', q)$  : transmission cross-coefficients  
 $\implies$  is approximated by a transfer function  $\tilde{T}(\vec{u})$  and several envelope functions  
(attenuation of a range of spatial frequencies)..

# Transfer function $\tilde{T}(\vec{u})$

Two cases:

→ **TEM** ( $\tilde{T}(\vec{u})$ : **T**ransfer **F**unction):

$$\tilde{\Psi}_i(\vec{u}) = \tilde{\Psi}_o(\vec{u}) \tilde{T}(\vec{u})$$

$$\Psi_i(\vec{x}) = \int \tilde{\Psi}_o(\vec{u}) \tilde{T}(\vec{u}) e^{2\pi i \vec{u} \cdot \vec{x}} d\vec{u}$$

→ **STEM** ( $\widetilde{OTF}(\vec{u}) = \tilde{T}(\vec{u}) \otimes \tilde{T}(-\vec{u})$ : **O**ptical **T**ransfer **F**unction):

$$I(\vec{x}) = \langle \Psi_i(\vec{x}; t) \Psi_i^*(\vec{x}; t) \rangle$$

$$\Psi_i(\vec{x}; t) = \Psi_o(\vec{x}; t) \otimes T(\vec{x})$$

$$I(\vec{x}) = \langle [\Psi_o(\vec{x}; t) \otimes T(\vec{x})] [\Psi_o^*(\vec{x}; t) \otimes T^*(\vec{x})] \rangle \quad (\otimes \text{ convolution.})$$

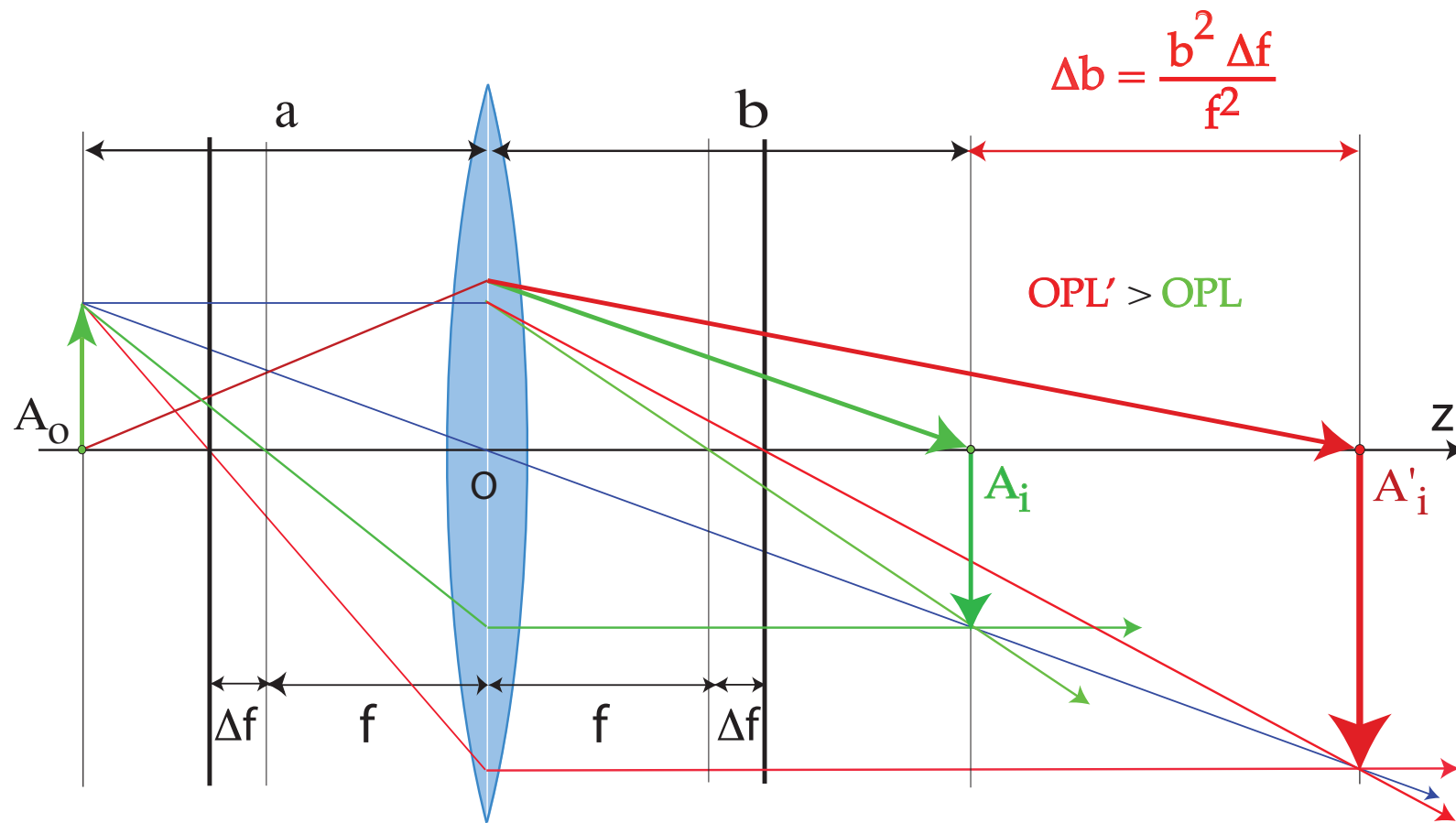
$$I(\vec{x}) = [T(\vec{x}) T^*(\vec{x})] \otimes \langle \Psi_o(\vec{x}; t) \Psi_o^*(\vec{x}; t) \rangle \quad (T(\vec{x}) \text{ is time independent.})$$

$$\langle \Psi_o(\vec{x}; t) \Psi_o^*(\vec{x}; t) \rangle = |\Psi_o(\vec{x})|^2 \quad (\text{complete spatial incoherence})$$

$$I(\vec{x}) = |\Psi_o(\vec{x})|^2 \otimes [T(\vec{x}) T^*(\vec{x})]$$

$$I(\vec{x}) = I_o(\vec{x}) \otimes OTF(\vec{x})$$

# Optical Path Length: underfocus



Underfocus weakens the objective lens, i.e. increases  $f$ . As a consequence the OPL from  $A_o$  to  $A'_i$  is larger:

$$e^{2\pi i \frac{\Delta f \lambda (\vec{q} \cdot \vec{q})}{2}}$$

$$T(\vec{q}) = e^{i\chi(\vec{q})} = \cos(\chi(\vec{q})) + i \underbrace{\sin(\chi(\vec{q}))}_{\text{Contrast transfer function}}$$

$$\chi(\vec{q}) = \pi \left[ W_{20} \lambda \vec{q} \cdot \vec{q} + W_{40} \frac{\lambda^3 (\vec{q} \cdot \vec{q})^2}{2} + \dots \right]$$

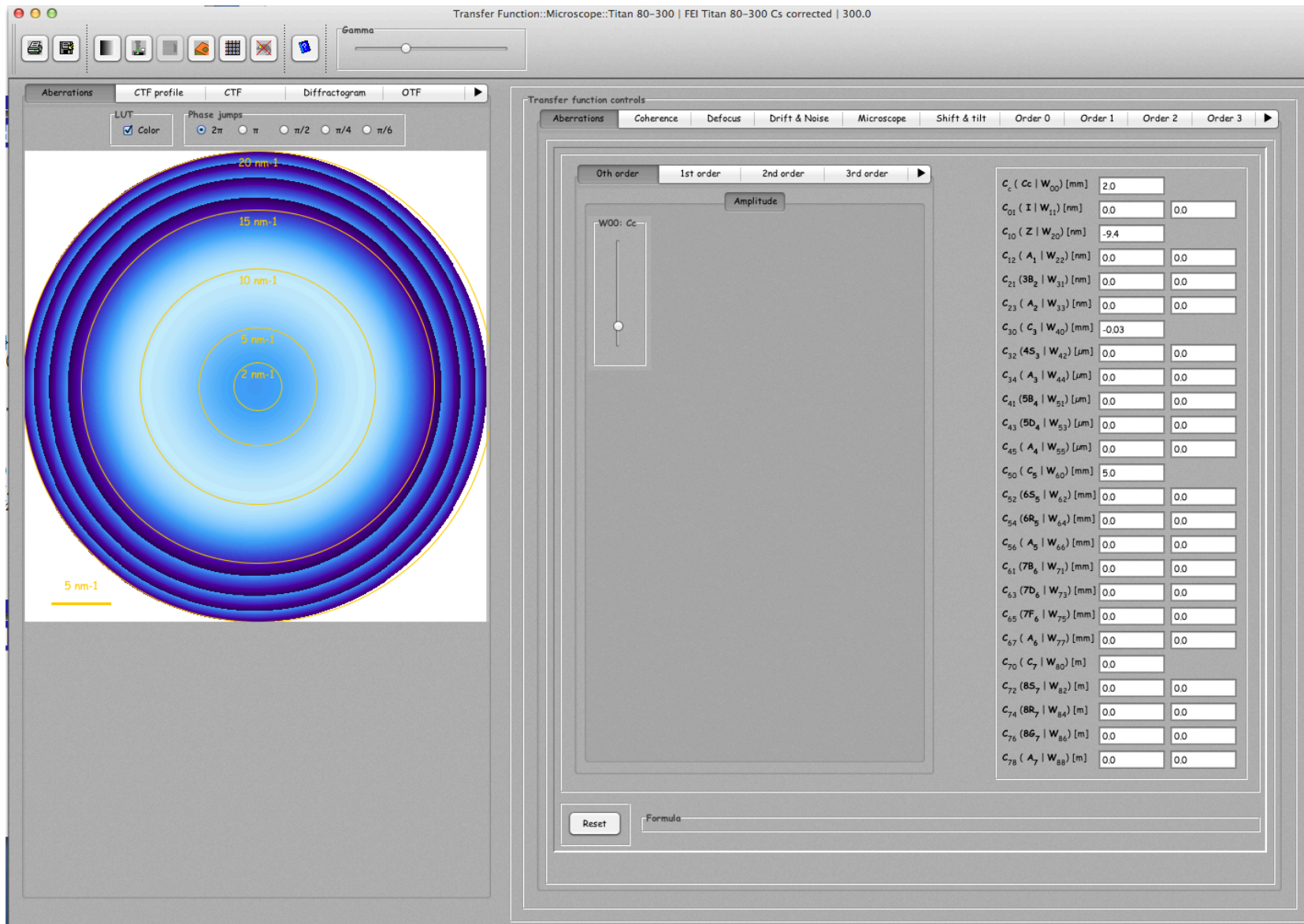
Where:

- ▶  $W_{20}$  : defocus ( $z$ )
- ▶  $W_{40}$ : spherical aberration ( $C_s$ )

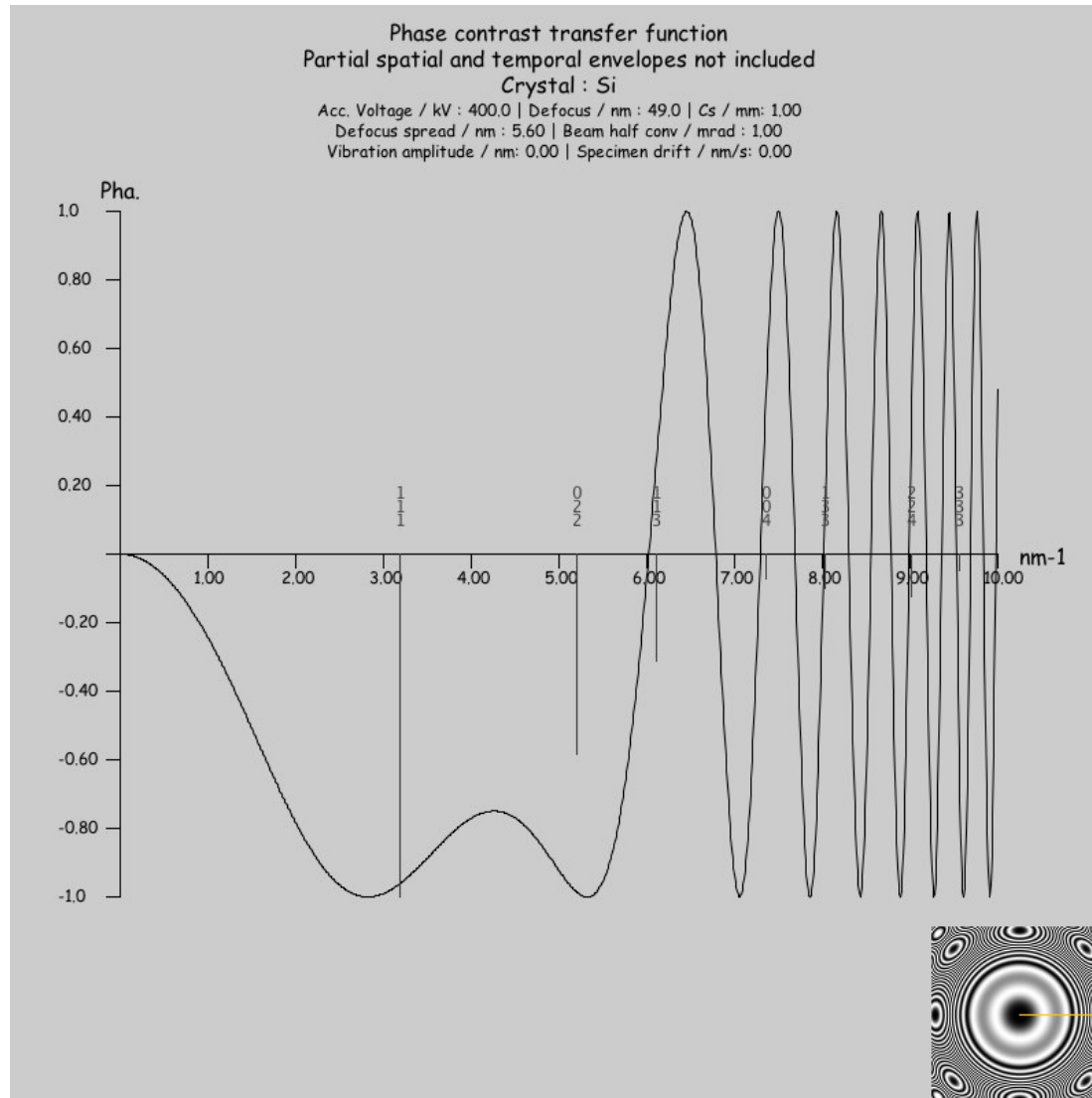
# Wavefront aberrations to 6<sup>th</sup> order (cartesian coordinates)

$$\begin{aligned}
 & \{z, \pi (u^2 + v^2) \lambda\} \text{ (defocus)} \\
 & \{W(1, 1), 2\pi(u \cos(\phi(1, 1)) + v \sin(\phi(1, 1)))\} \\
 & \{W(2, 2), \pi\lambda((u - v)(u + v) \cos(2\phi(2, 2)) + 2uv \sin(2\phi(2, 2)))\} \\
 & \{W(3, 1), \frac{2}{3}\pi (u^2 + v^2) \lambda^2(u \cos(\phi(3, 1)) + v \sin(\phi(3, 1)))\} \\
 & \{W(3, 3), \frac{2}{3}\pi\lambda^2 (u (u^2 - 3v^2) \cos(3\phi(3, 3)) - v (v^2 - 3u^2) \sin(3\phi(3, 3)))\} \\
 & \left\{ W(4, 0), \frac{1}{2}\pi (u^2 + v^2)^2 \lambda^3 \right\} \text{ (3<sup>rd</sup> order spherical aberration or } C_3) \\
 & \{W(4, 2), \frac{1}{2}\pi (u^2 + v^2) \lambda^3((u - v)(u + v) \cos(2\phi(4, 2)) + 2uv \sin(2\phi(4, 2)))\} \\
 & \{W(4, 4), \frac{1}{2}\pi\lambda^3 ((u^4 - 6v^2u^2 + v^4) \cos(4\phi(4, 4)) + 4u(u - v)v(u + v) \sin(4\phi(4, 4)))\} \\
 & \left\{ W(5, 1), \frac{2}{5}\pi (u^2 + v^2)^2 \lambda^4(u \cos(\phi(5, 1)) + v \sin(\phi(5, 1))) \right\} \\
 & \{W(5, 3), \frac{2}{5}\pi (u^2 + v^2) \lambda^4 (u (u^2 - 3v^2) \cos(3\phi(5, 3)) - v (v^2 - 3u^2) \sin(3\phi(5, 3)))\} \\
 & \{W(5, 5), \frac{2}{5}\pi\lambda^4 (u (u^4 - 10v^2u^2 + 5v^4) \cos(5\phi(5, 5)) + v (5u^4 - 10v^2u^2 + v^4) \sin(5\phi(5, 5)))\} \\
 & \left\{ W(6, 0), \frac{1}{3}\pi (u^2 + v^2)^3 \lambda^5 \right\} \text{ (5<sup>th</sup> order spherical aberration or } C_5) \\
 & \left\{ W(6, 2), \frac{1}{3}\pi (u^2 + v^2)^2 \lambda^5((u - v)(u + v) \cos(2\phi(6, 2)) + 2uv \sin(2\phi(6, 2))) \right\} \\
 & \left\{ W(6, 4), \frac{1}{3}\pi\lambda^5 ((u^6 - 5v^2u^4 - 5v^4u^2 + v^6) \cos(4\phi(6, 4)) + 4uv (u^4 - v^4) \sin(4\phi(6, 4))) \right\} \\
 & \left\{ W(6, 6), \frac{1}{3}\pi\lambda^5 ((u^6 - 15v^2u^4 + 15v^4u^2 - v^6) \cos(6\phi(6, 6)) + 2uv (3u^4 - 10v^2u^2 + 3v^4) \sin(6\phi(6, 6))) \right\}
 \end{aligned}$$

jems describes wavefront aberrations to order 8.



# Contrast transfer function: $\sin(\chi(\vec{q}))$



The transfer function of the objective lens in the absence of lens current and accelerating voltage fluctuations (Scherzer defocus). The (111) and (022) reflections of Si are phase shifted by  $-\frac{\pi}{2} \rightarrow$  black atomic columns.



In the **W**eak **P**hase **O**bject **A**pproximation under **optimum transfer conditions** the image intensity  $I(\vec{x})$  is:

- ▶ positive  $C_s$  (black atomic columns)

$$I(\vec{x}) \sim 1 - 2\sigma V_p(\vec{x})$$

- ▶ negative  $C_s$  (white atomic columns)

$$I(\vec{x}) \sim \sigma V_p(\vec{x})$$

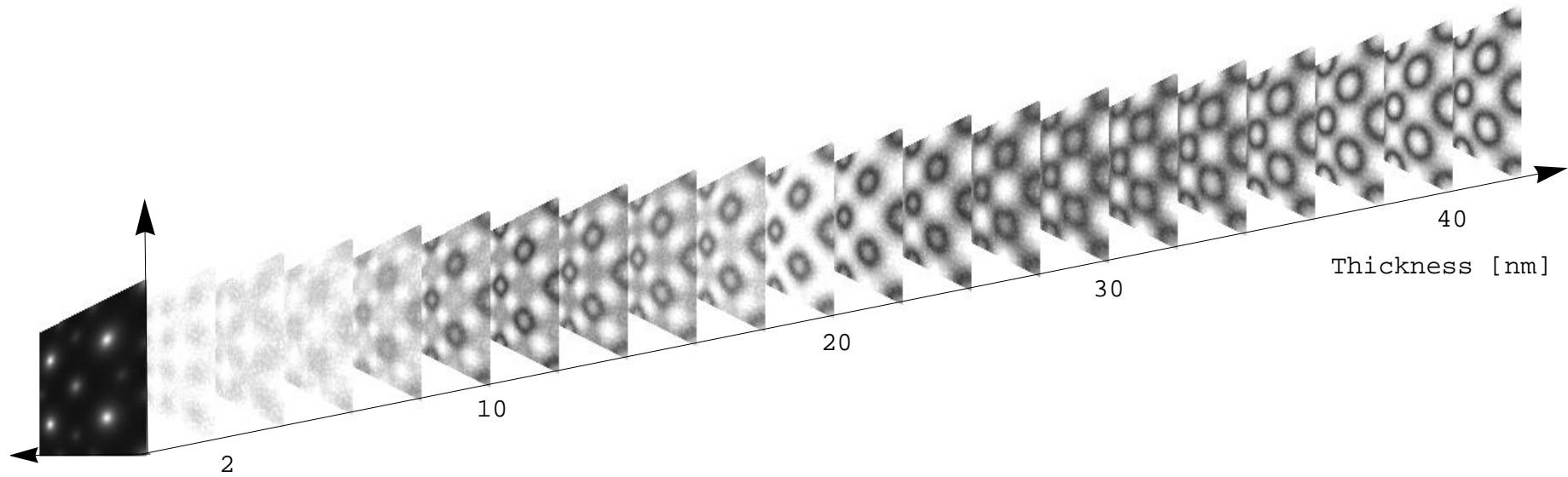
Where:

$V_p(\vec{x})$  : projected potential

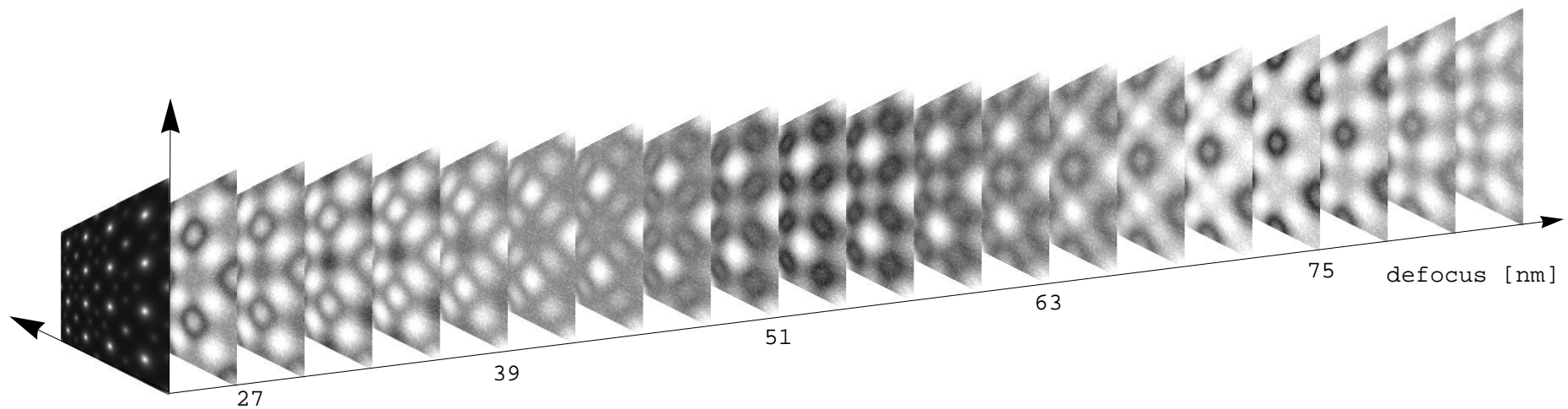
$\sigma$  : electron matter interaction constant

# HRTEM image depends on specimen thickness and object defocus

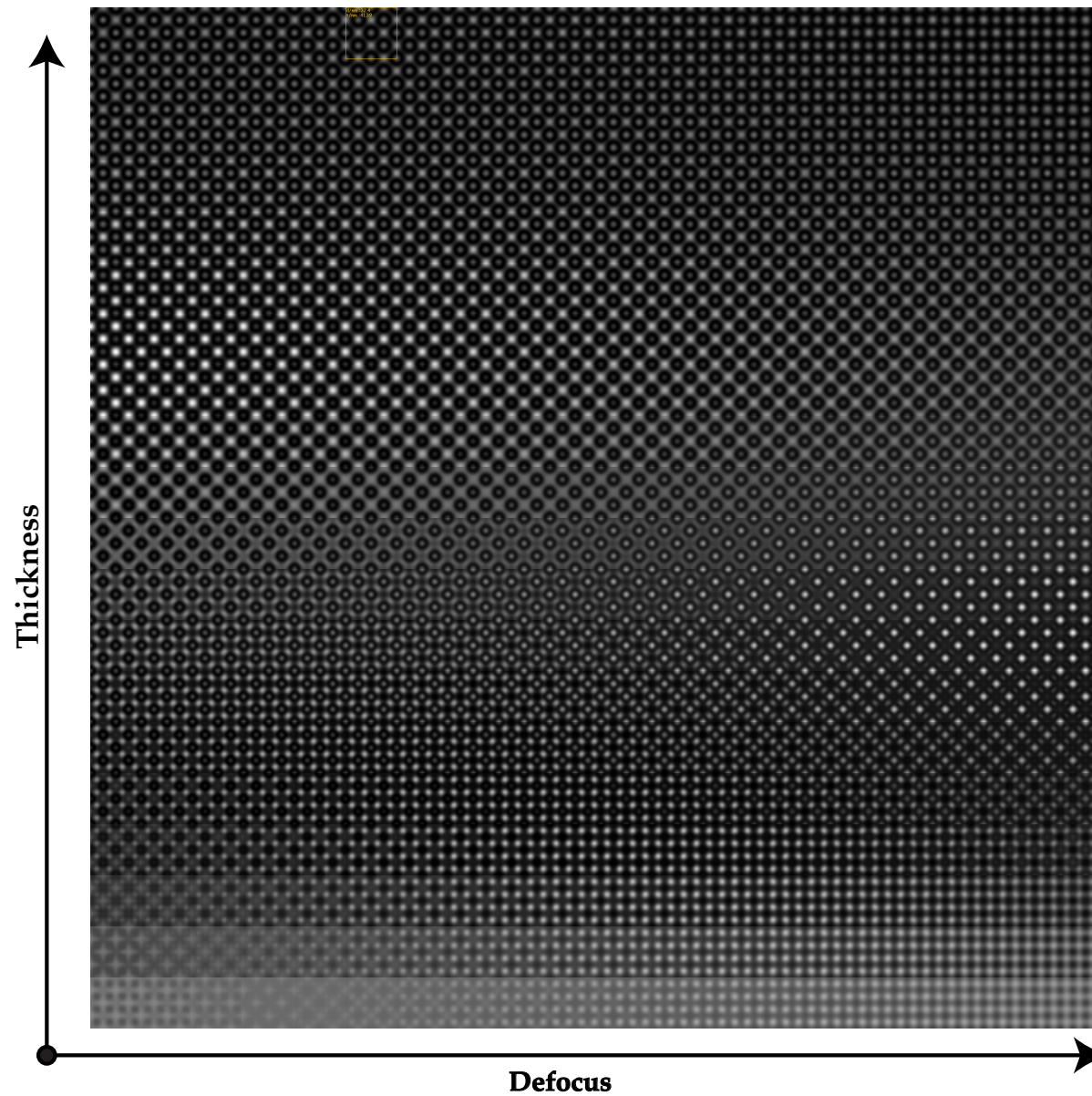
## Thickness series



## Defocus series



# Si [001] images map: contrast dependence of defocus & thickness



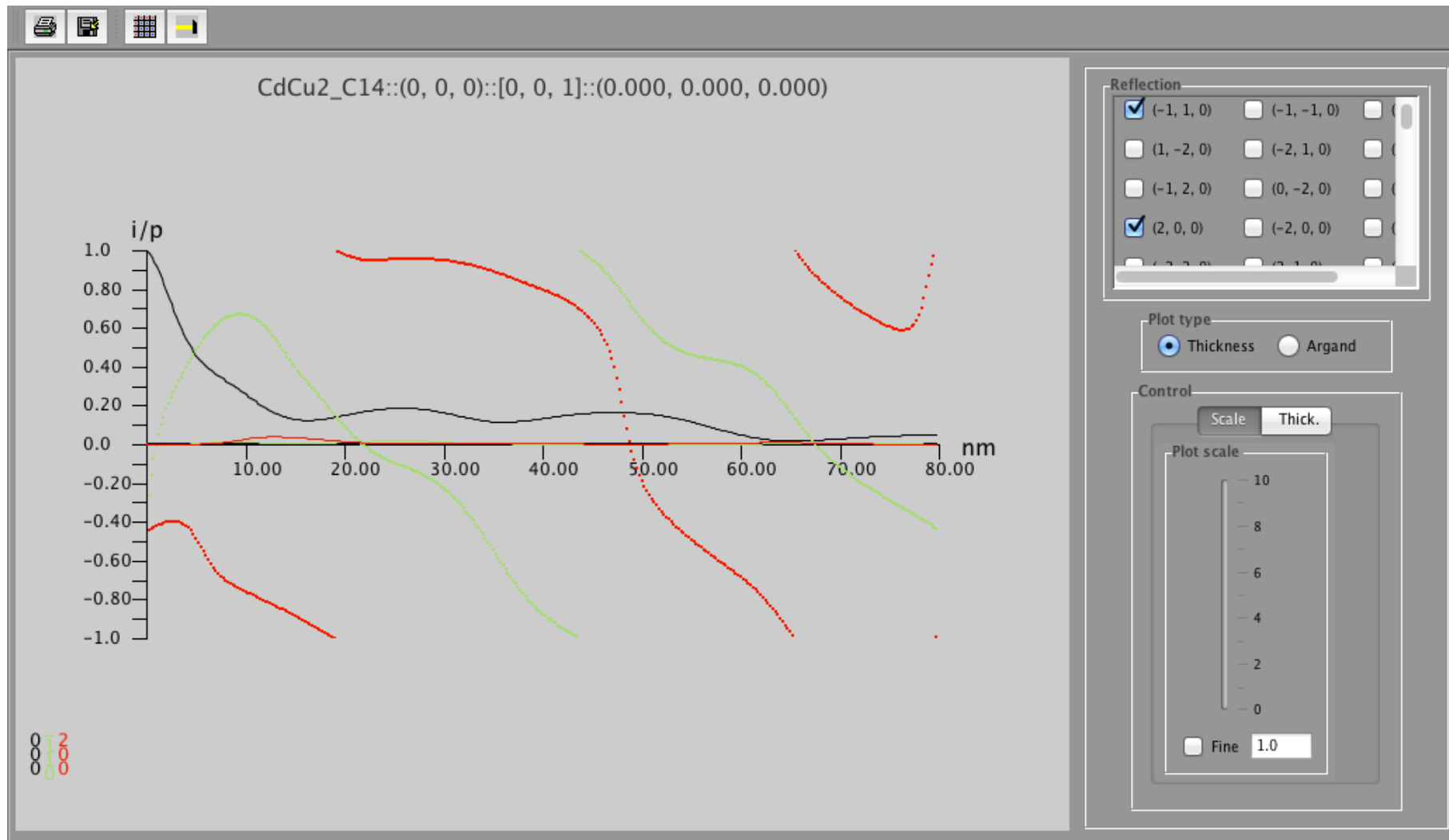
HREM map does not include the Modulation Transfer Function (MTF) of the detector.

# Problems

- ▶ Object
  - ▶ → Atomic scattering amplitude below 50 kV?
  - ▶ → Potential by DFT calculation?
  - ▶ ...
- ▶ HRTEM → Phase of diffracted beams evolves with specimen thickness.
- ▶ HRTEM → MTF of image acquisition system (Stobbs factor?).
- ▶ HRTEM / HRSTEM → Electron channeling depends on atomic column content.
- ▶ HRTEM / HRSTEM → Aberrations of optical system.
- ▶ HRTEM → Inelastic scattering (J.M. Cowley, E.J. Kirkland, D. van Dyck, A. Rosenaurer, K. Ishizuka, Z.L. Wang, H. Rose, H. Mueller, L. Allen, ...).
- ▶ HRTEM / HRSTEM → Drift, vibration, Johnson-Nyquist noise<sup>16</sup>, ...
- ▶ ...

<sup>16</sup>S. Uhlemann, H. Mueller, P. Hartel, J. Zach & M. Haider, Phys. Rev. Lett. **111** (2013) 046101.

# HRTEM problem: amplitude and phase of diffracted beams



Note that phase of diffracted beam is  $\frac{\pi}{2}$  out-of-phase with respect to transmitted beam.

# HRTEM problem: CCD MTF (Gatan MSC 1K x 1K, 24 $\mu\text{m}$ )

To make quantitative comparison with experimental HRTEM images the MTF of the detector must be introduced in the simulation.

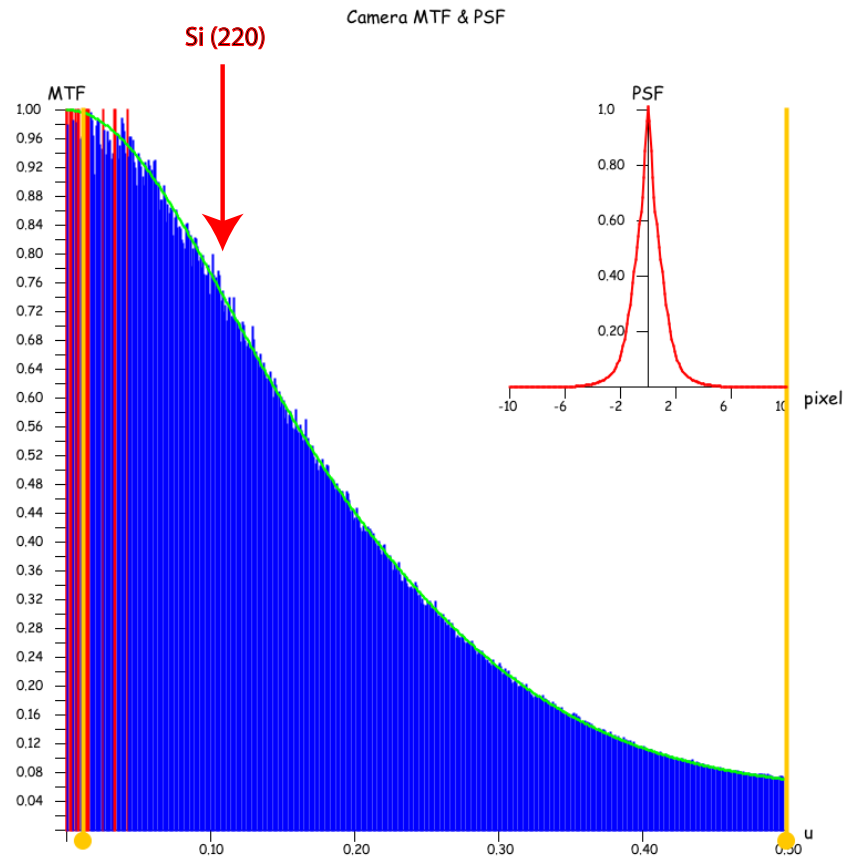


Figure: At high magnification Si (220) planes imaged with high contrast.

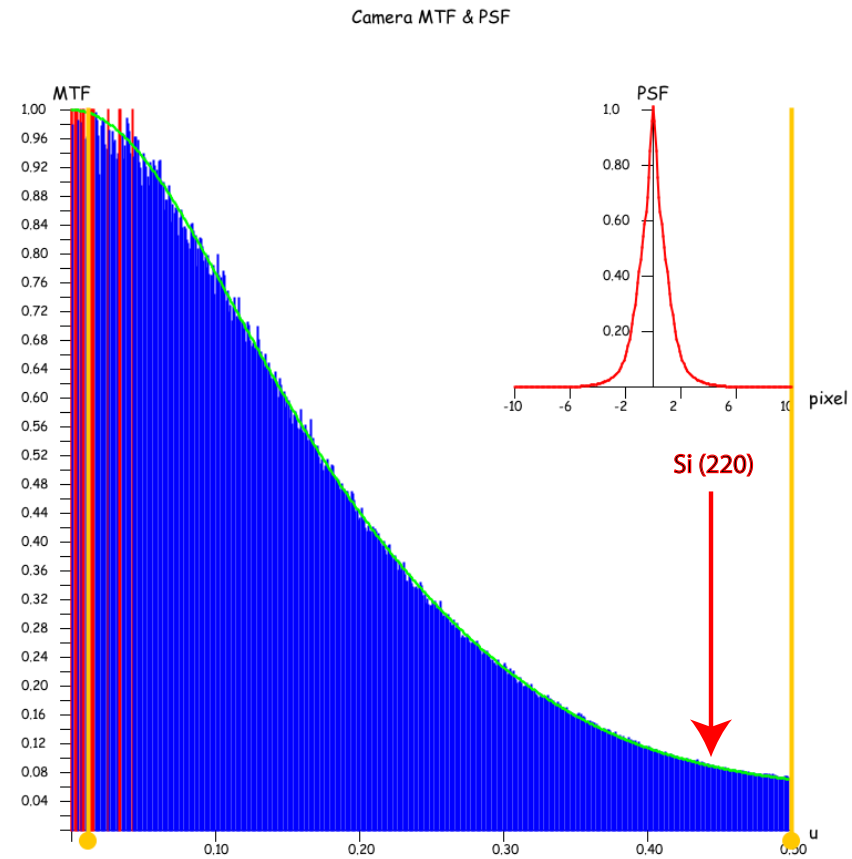


Figure: At low magnification Si (220) planes imaged with low contrast.

For quantitative comparison always use highest possible magnification (or include CCD MTF in simulations)!

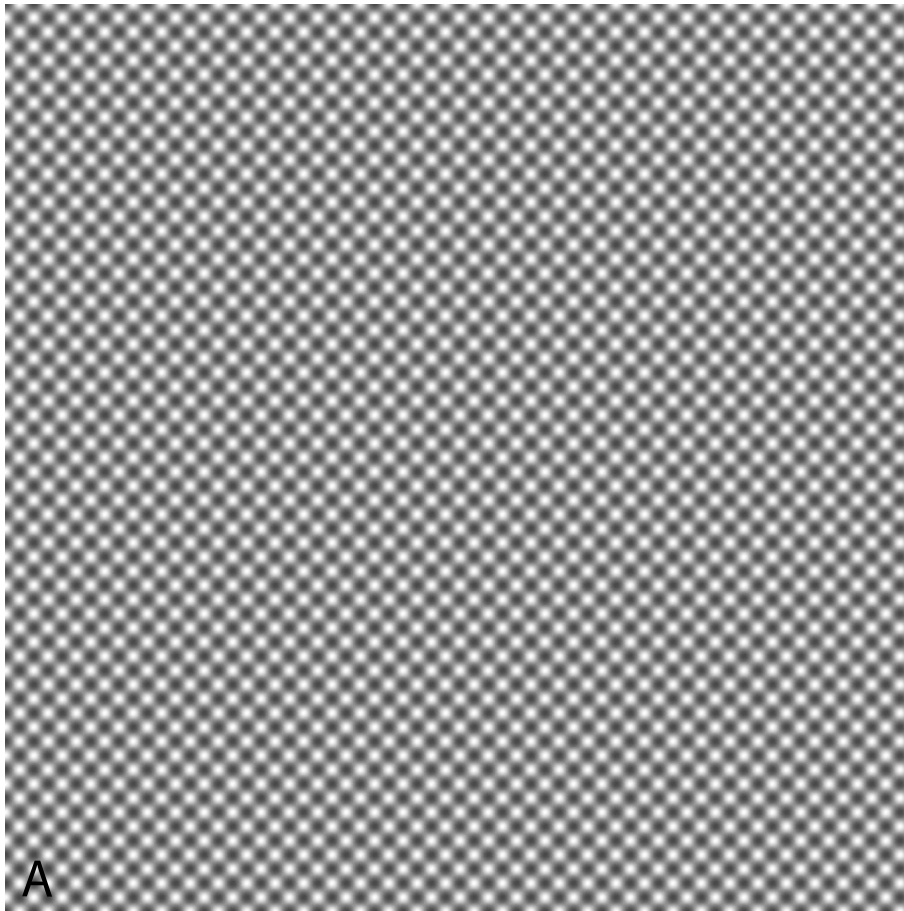


Figure: A: Si [001] simulation.

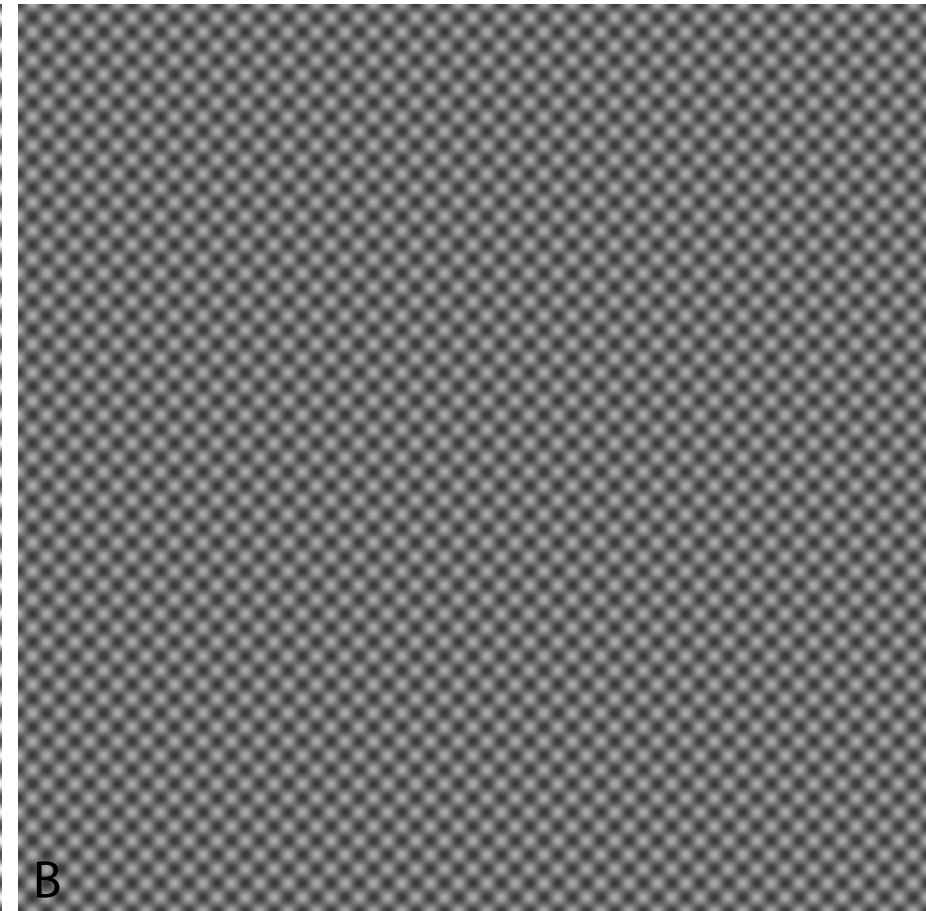


Figure: B: Si [001], simulation + CCD MTF.



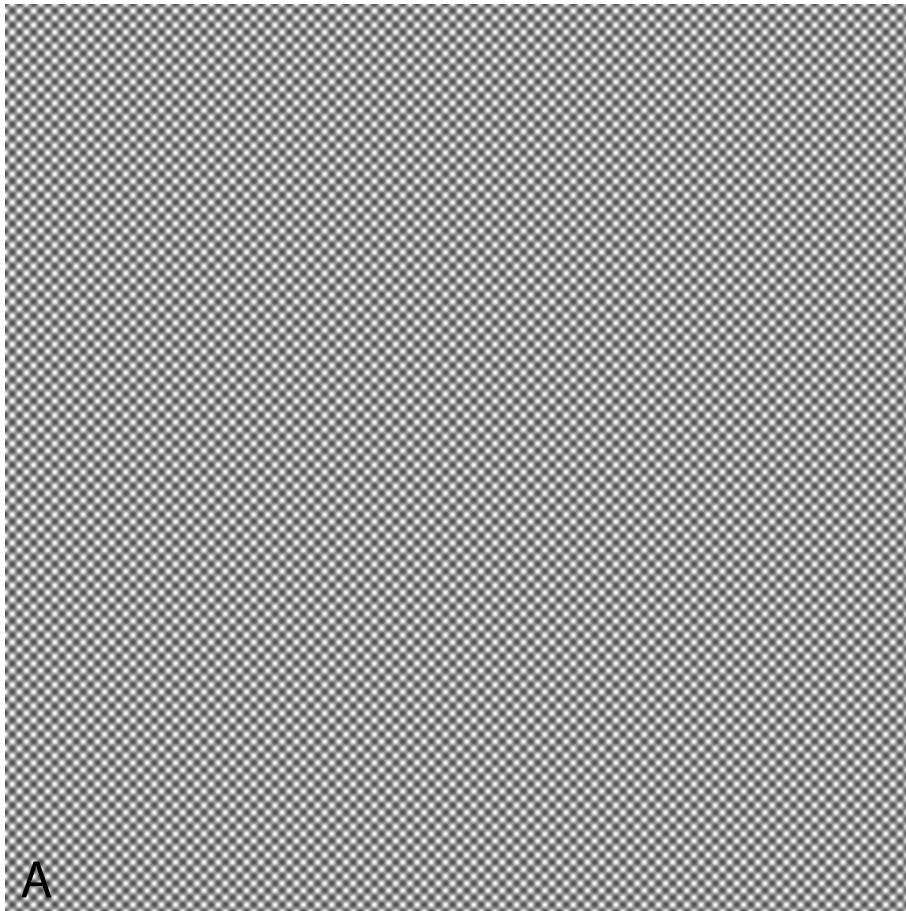


Figure: A: Si [001] simulation.

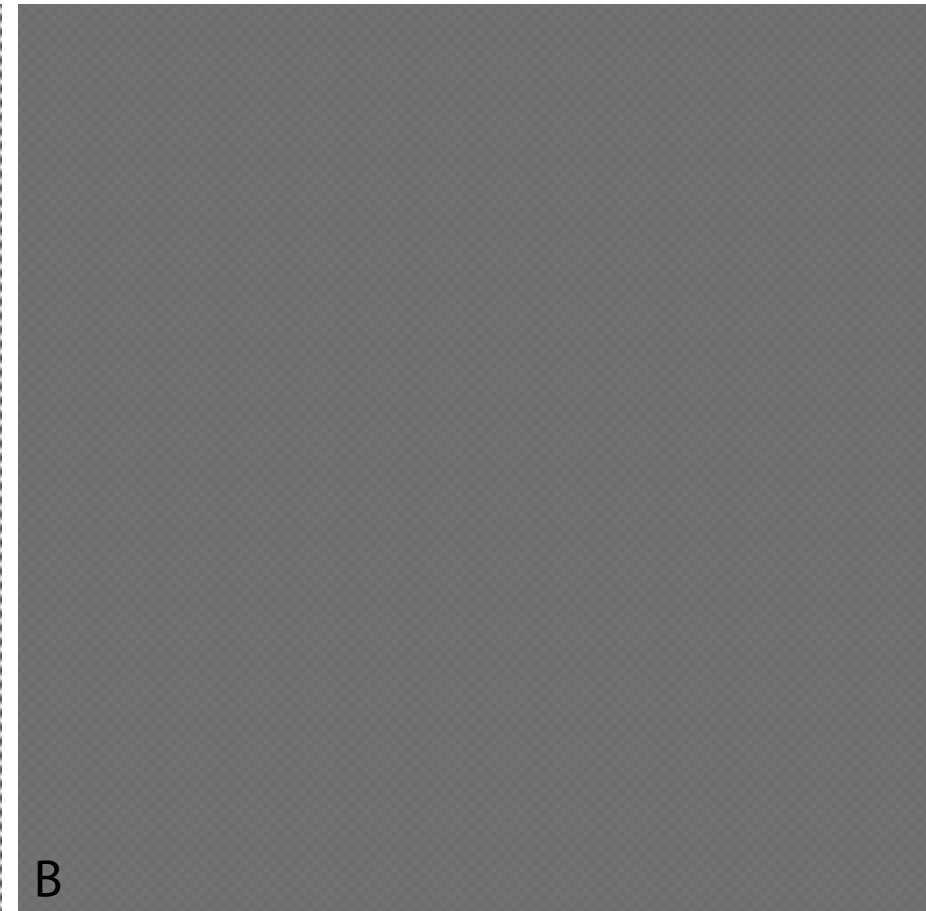


Figure: B: Si [001], simulation + CCD MTF.

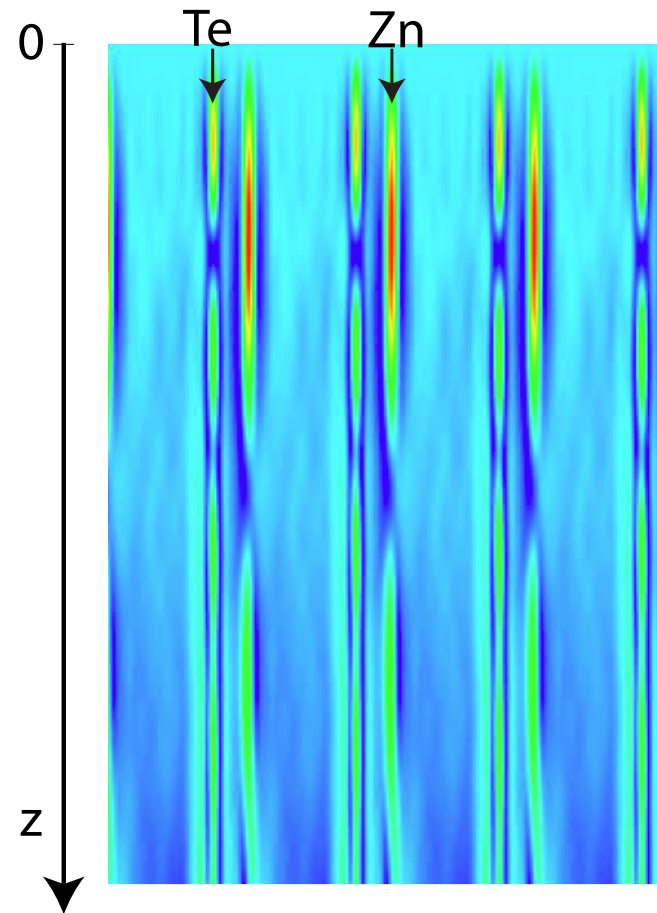
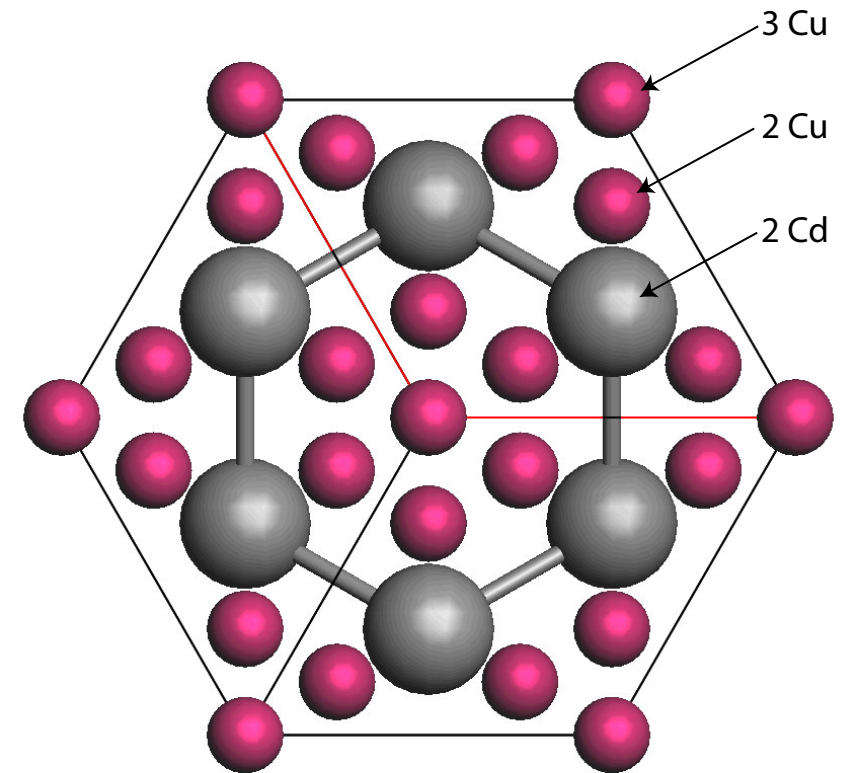
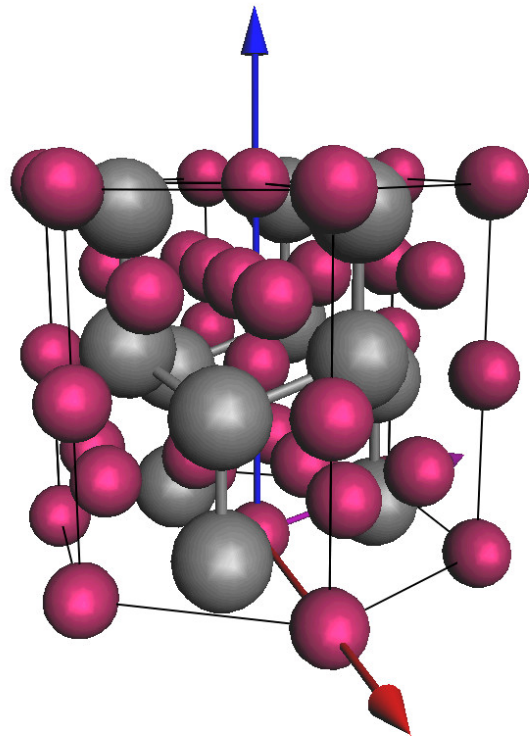


Figure: ZnTe [110] wave function intensity.

Channeling explains several features of HRTEM and STEM images (i.e. appearance / disappearance of contrast of impurities).

# Does $C_s$ and $C_c$ correction solves all imaging problems?

Example:  $\text{CdCu}_2$ , visibility of the 3 Cu atomic columns.

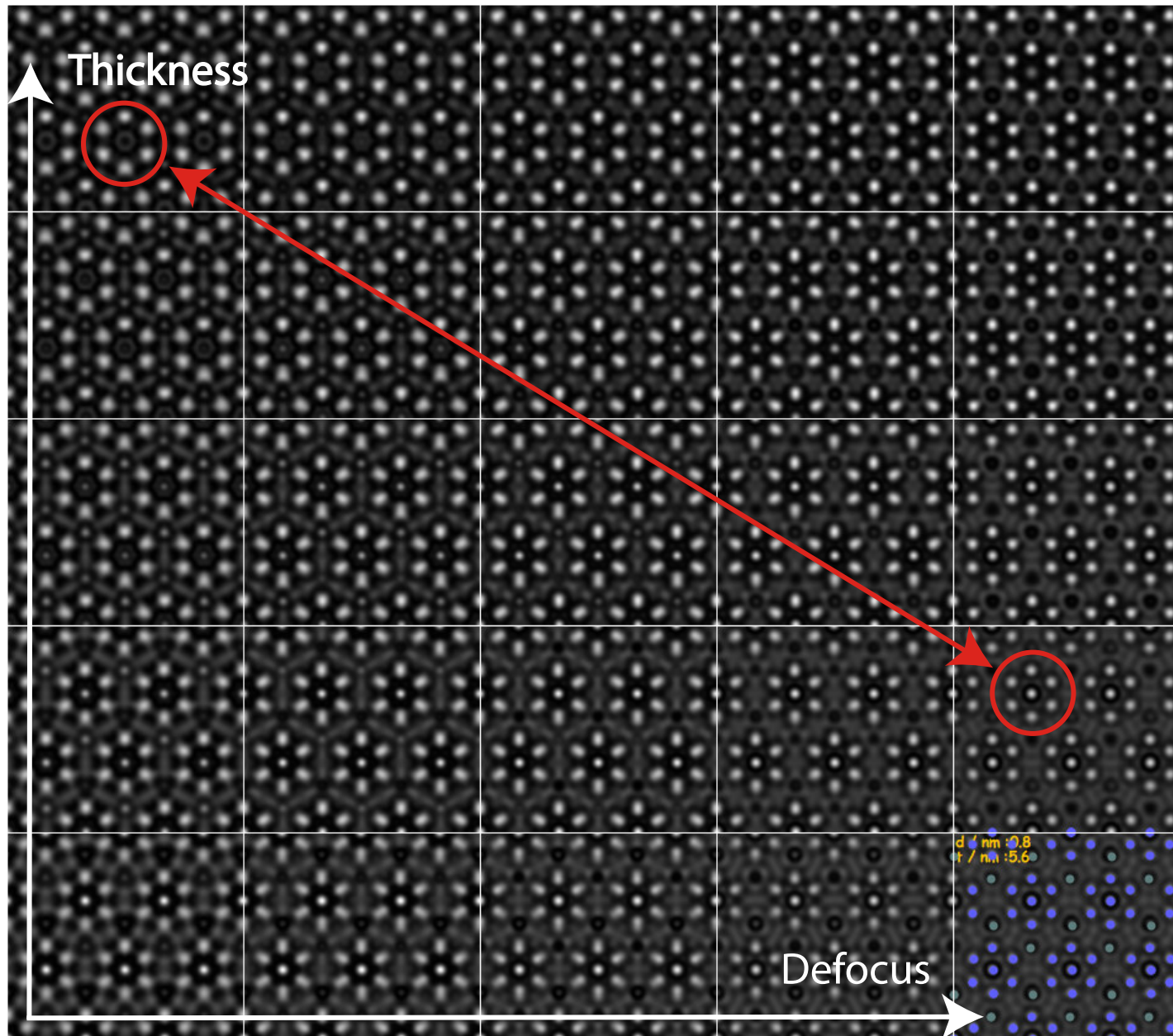


## *HRTEM image simulation conditions*

Acc. [kV]	$C_s$ [mm]	$C_5$ [mm]	$C_c$ [mm]	$\Delta E$ [eV]	Z [nm]	$\Delta z$ [nm]
300	-0.008	30	0.5	0.6	-4.9	1
300	-0.008	30	0.1	0.2	-2.0	1

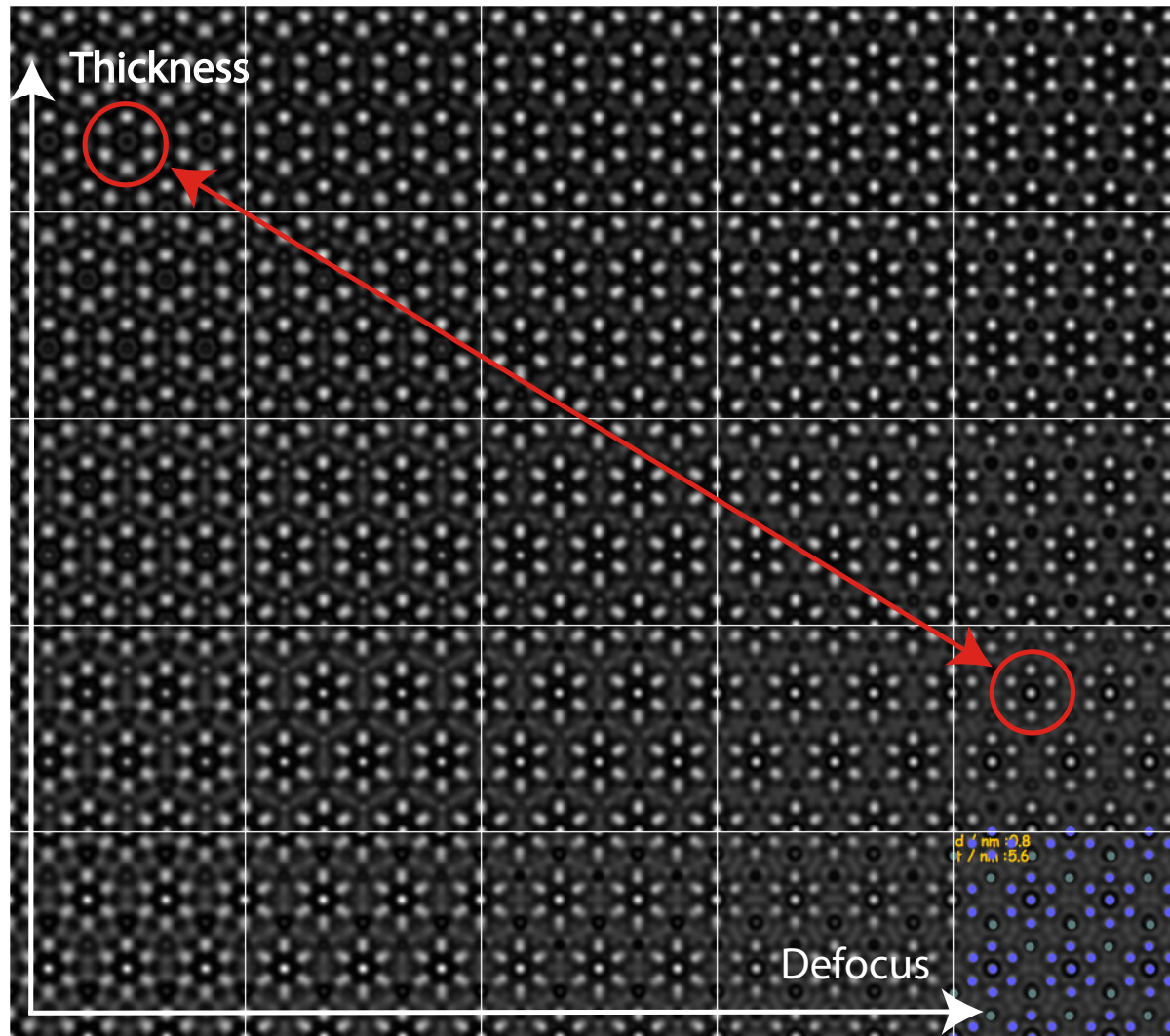
Dynamical scattering effects are not affected by  $C_s$  and/or  $C_c$  corrected TEM!

# $CdCu_2[001]$ : imaging parameters set 1



Visibility of 3 Cu atomic columns depends on specimen thickness and defocus.

# $CdCu_2[001]$ : imaging parameters set 2



Improving  $C_c$  and  $\Delta E$  does not affect the visibility of 3 the Cu atomic columns. It depends on specimen thickness (and defocus indeed). Visibility of the 3 Cu atomic columns is **always** affected by dynamical scattering. Only extremely thin specimen ( $\leq 10$  nm) will allow **faithful** imaging of crystal projected potential.

High Angle Annular Dark Field (HAADF): inelastically scattered electrons.

When simulation is necessary how to simulate images?

Numerous approximations:

- ▶ Simple projected + convolution with probe intensity: no channeling effect (**Weak Object Approximation**).
- ▶ Multislice calculation: channeling + inelastic scattering (absorption potential) + convolution with probe intensity.
- ▶ Frozen lattice (phonon) approximation: atoms of super-cell displaced out of equilibrium position, probe scanned on imaged area, intensity collected by annular detector.
- ▶ Pennycook, Nellist, Ishizuka, Shiojiri, Allen, Wang, Rosenauer, van Dyck, ...

Except the first 2 methods, simulation time expensive (**luxury?**). Approximations (**necessity**) may suffice...

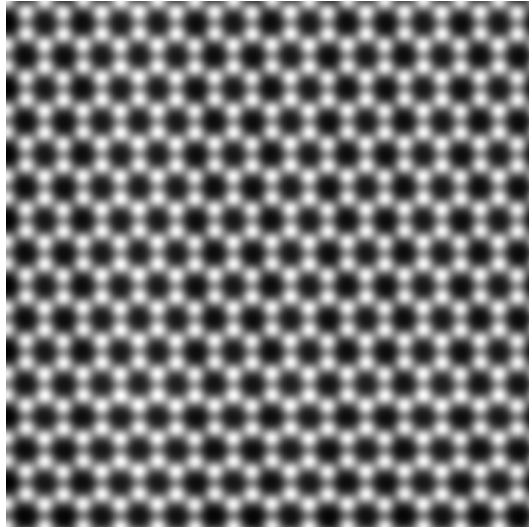


Figure: Proj. pot. approx.



Figure: Channeling calculation.

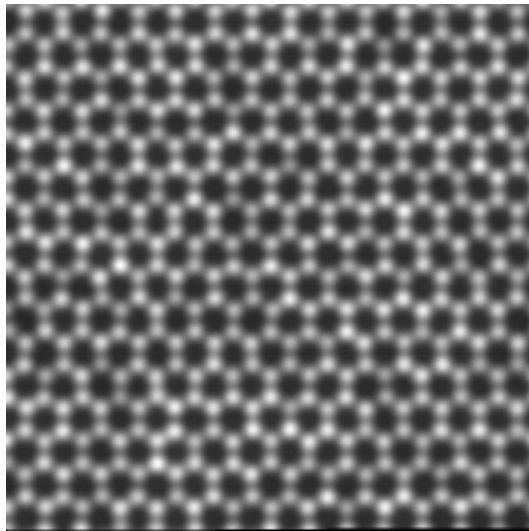


Figure: Frozen lattice 5 conf.

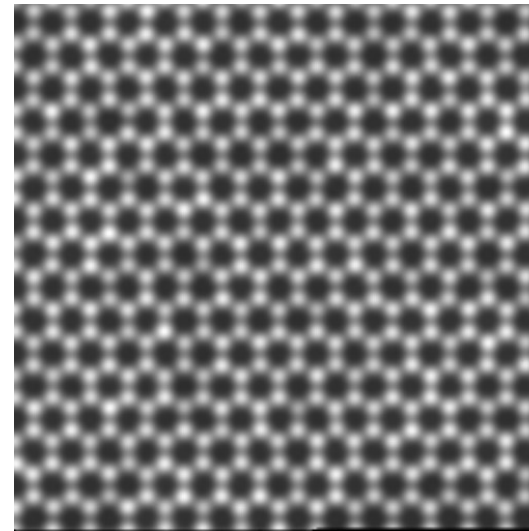


Figure: Frozen lattice 10 conf.

# HRSTEM - HRTEM comparison: graphene with add atoms

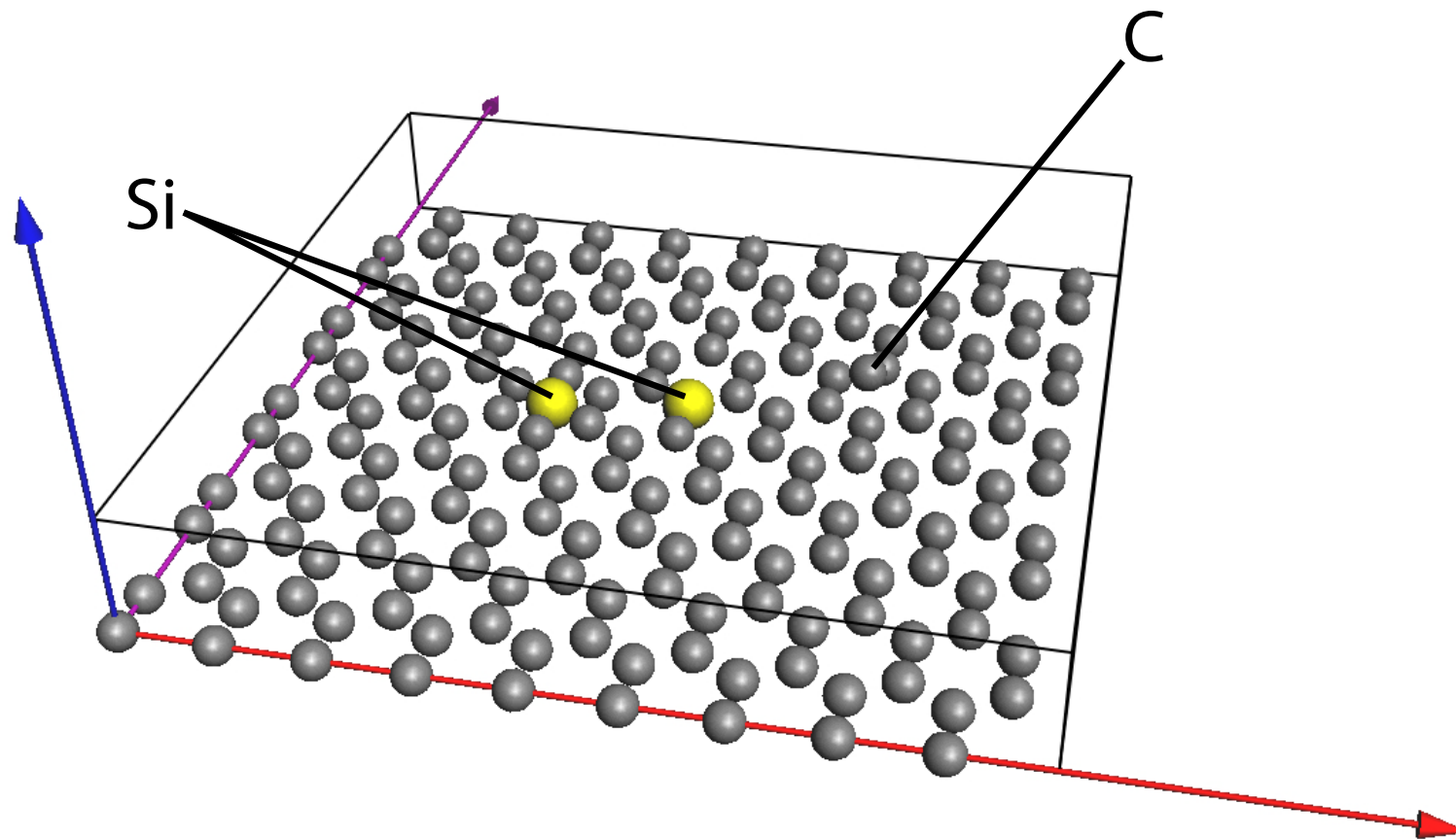


Figure: Graphene with Si in 6 C ring, Si substitutional and 2 C column.





Figure: Frozen lattice ( $\sim 400$  s).



Figure: Channeling ( $\sim 2$  s).

One Si shows more contrast than 2 C atoms ( $i \sim Z^2$ ) :  $14^2$   
compared to  $\sim 2 \times 6^2$ .

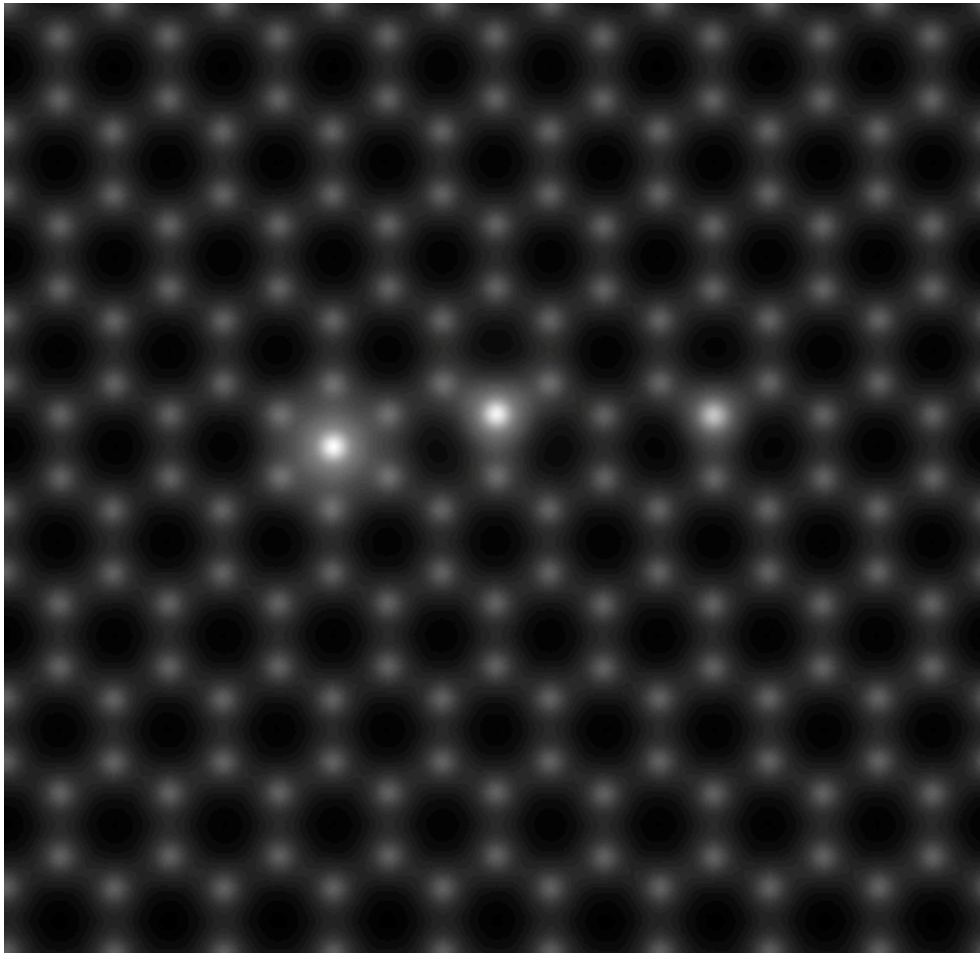


Figure: Weak phase object app.,  $C_c = 0.5\text{mm}$

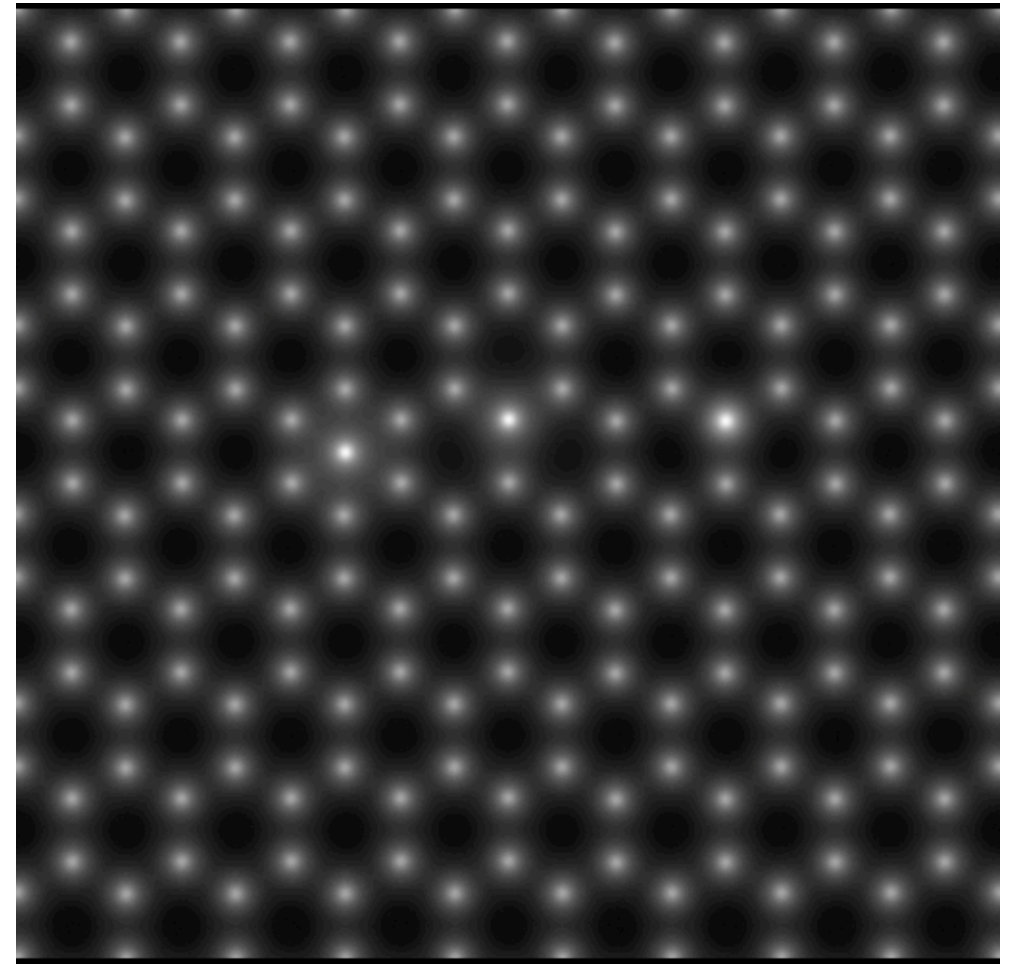


Figure: Multislice,  $C_s = -0.033\text{mm}$ ,  $C_c = 0$ , no thermal magnetic noise.

HRTEM does not display the strong contrast difference between one Si and two C as given by HAADF.

Image simulation necessary for quantitative work<sup>17</sup>.

- ▶ Exit wave function recovery using focal series reconstruction.
- ▶ Transport of intensity equation.

But... can also be used for teaching or  
planning HRTEM/HRSTEM  
observations.

<sup>17</sup>K. W. Urban, Science **321** (2008) 506.

Reaching 0.05 nm resolution sets very strong conditions on aberrations correction.

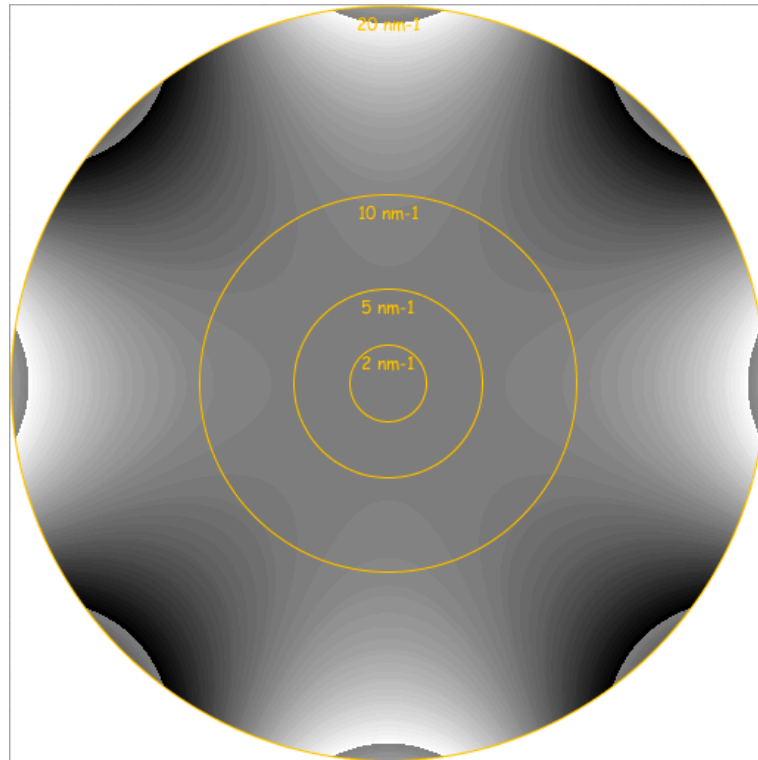


Figure: Aberration figure of  $C_{34}(0.5\mu\text{m})$ , phase jump at  $\frac{\pi}{4}$ .

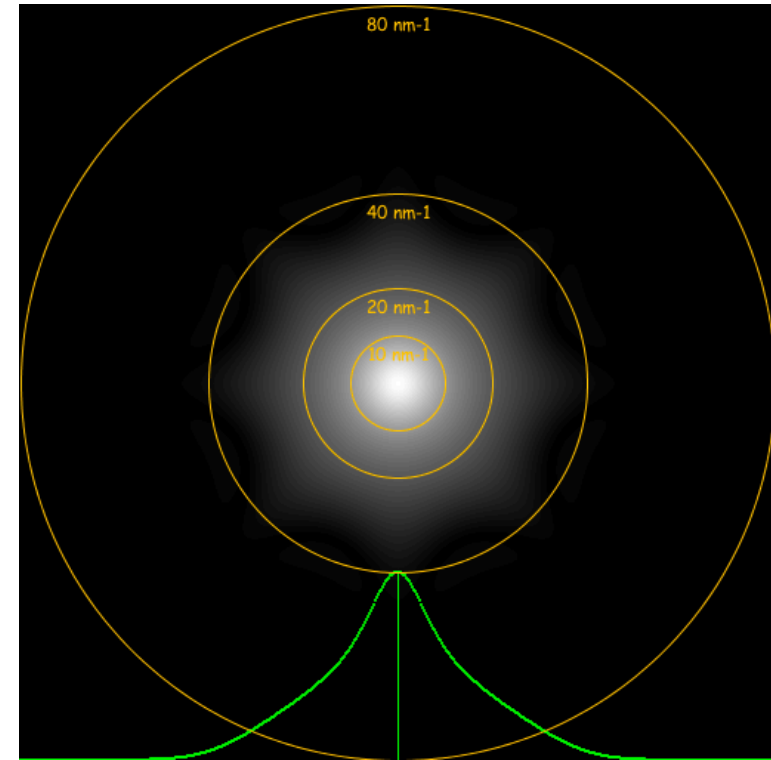


Figure: Optical Transfer Function.

Note that Optical Transfer Function (HRSTEM) transfers higher spatial frequencies than Coherent Transfer Function (HRTEM).

# HAADF: graphene

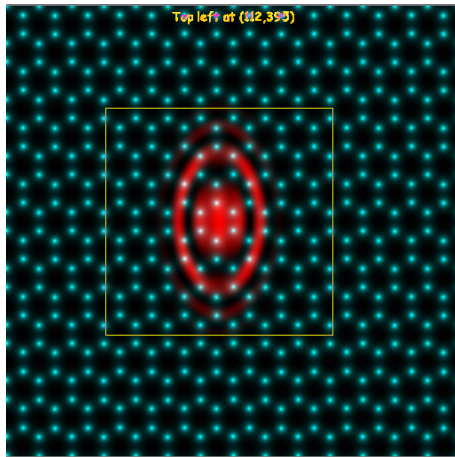


Figure: Probe affected by 2 fold astigmatism.

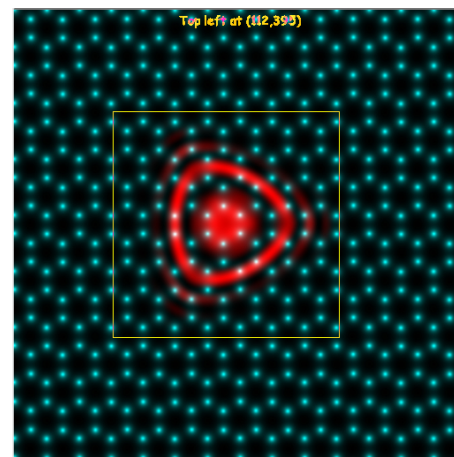


Figure: Probe affected by 3 fold astigmatism.

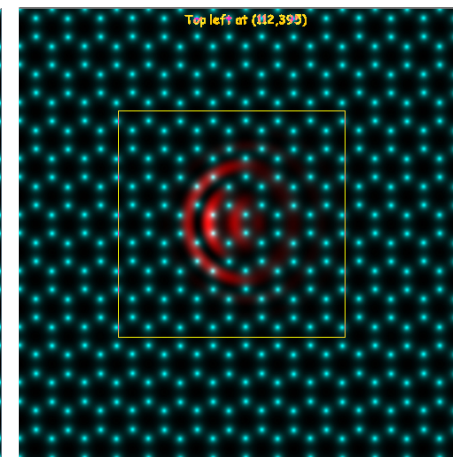


Figure: Probe affected by coma.

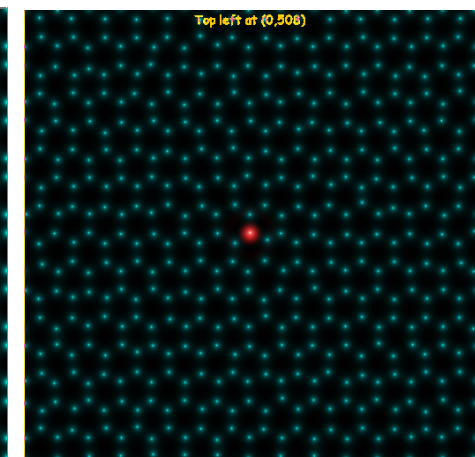


Figure: Corrected probe (best defocus).

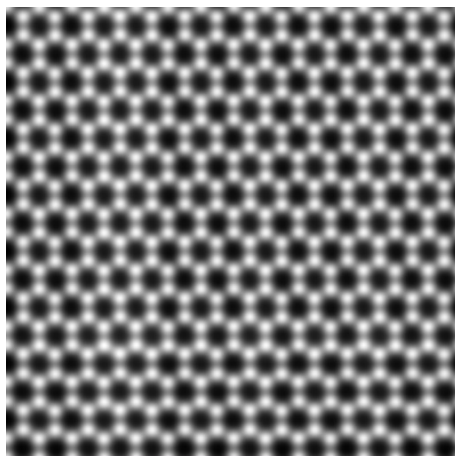


Figure: HAADF projected potential approximation.

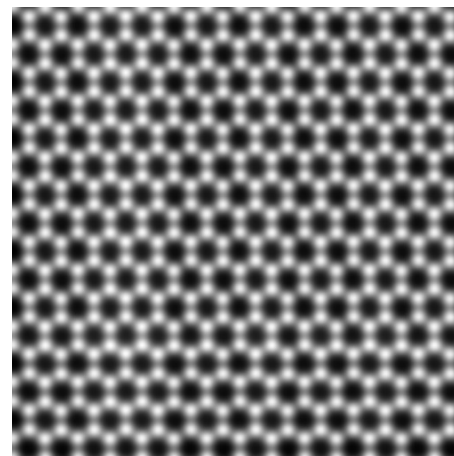


Figure: HAADF multislice calculation (simple).

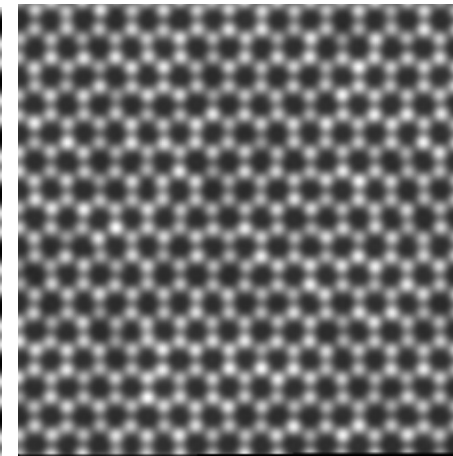


Figure: Frozen phonons 5 configurations.

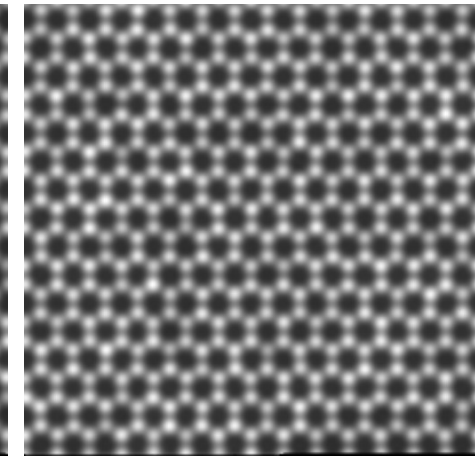


Figure: Frozen phonons 10 configurations.

# Appendix 1: Dynamical theory of elastic scattering of high energy electron

We aim to understand in details **multiple elastic scattering** of electrons by crystals.

- ▶ High energy electron ( $eE$ ).
- ▶ **Periodic** interaction potential  $V(\vec{r})$ .
- ▶ Time **independent** flux of incident electrons.

The **fundamental equation of electron elastic scattering** by a potential  $V_v$  [Volt] (positive inside a crystal) in the approximation of a stationary flux of electrons of a given energy  $eE$  is the **Schrödinger** equation ([?]):

$$\Delta \Phi(\vec{r}) + \frac{2me}{\hbar^2} [E + V_v(\vec{r})] \Phi(\vec{r}) = 0$$

With a change of notation its is written as:

$$[\Delta + 4\pi^2 K_i^2] \Phi(\vec{r}) = -4\pi^2 V_v(\vec{r}) \Phi(\vec{r})$$

Where the wavevector  $|\vec{K}_i|$  of the incident electrons is given by:

$$|K_i| = \frac{\sqrt{2meE}}{h}$$

and

$$m = \gamma m_0$$

# Schrödinger equation

The Laplacian  $\Delta = \frac{\partial^2}{\partial x^2} + \frac{\partial^2}{\partial y^2} + \frac{\partial^2}{\partial z^2}$  is written as:  $\Delta_\rho + \frac{\partial^2}{\partial z^2}$ . As a result,  $[\Delta + \dots]e^{2\pi i k_z z}\Psi(\rho; z)$  is given by:  $[\Delta_\rho + \frac{\partial^2}{\partial z^2} + \dots]e^{2\pi i k_z z}\Psi(\rho; z)$ .

Performing the z-differentiation:

$$\frac{\partial^2}{\partial z^2}e^{2\pi i k_z z}\Psi(\rho; z) = e^{2\pi i k_z z}[-4\pi^2 k_z^2 + 4\pi i k_z \frac{\partial}{\partial z} + \frac{\partial^2}{\partial z^2}]\Psi(\rho; z)$$

Inserting the last expression and dropping the term  $e^{2\pi i k_z z}$ :

$$[\Delta_\rho + 4\pi^2(K_i^2 - k_z^2 + V(\rho; z)) + 4\pi i k_z \frac{\partial}{\partial z} + \frac{\partial^2}{\partial z^2}]\Psi(\rho; z) = 0$$

Since  $K_i^2 = k_z^2 + \chi^2$ :

$$[\Delta_\rho + 4\pi^2\chi^2 + 4\pi^2 V(\rho; z) + 4\pi i k_z \frac{\partial}{\partial z} + \frac{\partial^2}{\partial z^2}]\Psi(\rho; z) = 0$$

Rearranging the last equation:

$$i \frac{\partial \Psi(\rho; z)}{\partial z} = -\frac{1}{4\pi k_z} [\Delta_\rho + 4\pi^2\chi^2 + 4\pi^2 V(\rho; z) + \frac{\partial^2}{\partial z^2}]\Psi(\rho; z)$$

# Fundamental equation

$$i \frac{\partial \Psi(\rho; z)}{\partial z} = -\frac{1}{4\pi k_z} [\Delta_\rho + 4\pi^2 \chi^2 + 4\pi^2 V(\rho; z) + \frac{\partial^2}{\partial z^2}] \Psi(\rho; z)$$

The term  $|\frac{\partial^2 \Psi(\rho; z)}{\partial z^2}|$  being **much smaller** than  $|k_z \frac{\partial \Psi(\rho; z)}{\partial z}|$  we drop it (this is equivalent to **neglect backscattering**).

Fundamental equation of **elastic scattering** of **high energy mono-kinetic electrons** with a potential within the approximation of **small angle scattering**:

$$i \frac{\partial}{\partial z} \Psi(\rho; z) = -\frac{1}{4\pi k_z} [\Delta_\rho + 4\pi^2 \chi^2 + 4\pi^2 V(\rho; z)] \Psi(\rho; z)$$

Time dependent Schrödinger equation  $\implies$  solution by many methods of quantum mechanics!



- ▶ The approximations of the fundamental equation are equivalent to assume that the **scattering potential is small compared to the accelerating potential** and that  $k_z$  varies only slightly with  $z$ . It is in fact a quite good approximation, since the mean crystal potential is of the order of  $10 - 20$  V.
- ▶ **Electron backscattering** is neglected, the electrons are moving forwards.
- ▶ The fundamental equation is actually equivalent to a **2-dimensional Schrödinger equation** ( $\rho = \{x, y\}$ ) where  $z$  plays the role of time. The system evolution is **causal**, from the past to the future.

Fundamental equation in **Hamiltonian** form:

$$i \frac{\partial}{\partial z} \Psi = H \psi$$

where:

$$H = -\frac{1}{4\pi k_z} [\Delta_\rho + 4\pi^2 \chi^2 + 4\pi^2 V(\rho; z)] = H_0 + \frac{4\pi^2 V(\rho; z)}{4\pi k_z}$$

A **fundamental postulate of quantum mechanics** ([?, ?]) says that the evolution operator obeys the equation:

$$i \frac{\partial}{\partial z} U(z, 0) = H(\rho; z) U(z, 0)$$

# Causal evolution operator

$U(z, 0)$ : **unitary operator** (the norm of  $|\Psi\rangle$  is conserved), in general not directly integrable  $\implies$  **approximations**.

$U(z, 0)$  can be **directly integrated** only when  $H(\rho; z)$  and  $\frac{\partial}{\partial z}H(\rho; z)$  commute. In that case the general solution is [?]:

$$U(z, 0) = e^{-i \int_0^z H(\tau) d\tau}$$

$H(\rho; z)$  and  $\frac{\partial}{\partial z}H(\rho; z)$  commute when:

- ▶  $V(\rho; z)$  does not depend on  $z$ , i.e.  $V(\rho; z) = V(\rho)$  (**perfect crystal**).
- ▶  $V(\rho; z)$  can be neglected (**free space propagation**).
- ▶  $H(\rho; z)$  is approximated by its potential term (**phase object**).

Three approximations are available in jems:

- ▶ **Multislice** method.
- ▶ **Bloch wave** method.
- ▶ **Howie-Whelan** column approximation.